HELICOPTER TURBOSHAFT ENGINE GROUND PERFORMANCE WITH ALTERNATIVE FUELS

A THESIS SUBMITTED TO
THE GRADUATE SCHOOL OF NATURAL AND APPLIED SCIENCE
OF
MIDDLE EAST TECHNICAL UNIVERSITY

BY

UFUK BAŞLAMİŞLİ

IN PARTIAL FULFILLMENT OF THE REQUIREMENTS
FOR
THE DEGREE OF MASTER OF SCIENCE
IN
AEROSPACE ENGINEERING

FEBRUARY 2012

Approval of the thesis:

HELICOPTER TURBOSHAFT ENGINE GROUND PERFORMANCE WITH ALTERNATIVE FUELS

submitted by **UFUK BAŞLAMİŞLİ** in partial fulfillment of the requirements for the degree of **Master of Science in Aerospace Engineering Department, Middle East Technical University** by,

Prof. Dr. Canan Özgen _____
Dean, Graduate School of **Natural and Applied Science**

Prof. Dr. Ozan Tekinalp _____
Head of Department**, Aerospace Engineering**

Prof. Dr. İ. Sinan Akmandor _____
Supervisor**, Aerospace Engineering Dept., METU**

Examining Committee Members:

Prof. Dr. Cevdet Çelenligil _____
Aerospace Engineering Dept., METU

Prof. Dr.İ. Sinan Akmandor _____
Aerospace Engineering Dept., METU

Assoc. Prof. Dr. Sinan Eyi _____
Aerospace Engineering Dept., METU

Asst. Prof. Dr. Oğuz Uzol _____
Aerospace Engineering Dept., METU

Asst. Prof. Dr. Ahmet Yozgatlıgil _____
Mechanical Engineering Dept., METU

Date: **03.02.2012**

I hereby declare that all information in this document has been obtained and presented in accordance with academic rules and ethical conduct. I also declare that, as required by these rules and conduct, I have fully cited and referenced all material and results that are not original to this work.

Name, Last Name: Ufuk BAŞLAMİŞLİ

Signature:

ABSTRACT

HELICOPTER TURBOSHAFT ENGINE GROUND PERFORMANCE WITH ALTERNATIVE FUELS

Başlamişli, Ufuk

M.Sc., Department of Aerospace Engineering

Supervisor: Prof. Dr. İ. Sinan Akmandor

February 2012, 79 pages

In recent years, extensive studies on alternative fuels have been conducted to find environmentally friendly, economically feasible fuels due to finite petroleum sources, environmental and economical reasons. In this thesis, effects of alternative fuels on engine performance and exhaust emission are studied experimentally. Cold and reacting tests have been performed. Volumetric flow rate, discharge pressure are measured according to different pump speed. Droplet diameters, droplet distribution, spray cone angle and two dimensional velocity distribution from combustor fuel nozzle are determined by IPI and PIV technique. The comparative performance of alternative fuels and JET A-1 are investigated by atmospheric combustion tests and experimental turbojet tests in terms of exhaust gas temperatures, emissions, combustion chamber efficiency. Emissions, combustion chamber exit temperature profile, power turbine inlet and exhaust gas temperatures, effects of fuels on engine performance are observed and measured in detail at RR Allison 250 C-18 turbo-shaft engine.

Keywords: Alternative Fuel, Emission, Turbo-shaft Engine, Helicopter Engine

ÖZ

ALTERNATİF YAKITLARLA HELİKOPTER TURBO-ŞAFT MOTOR YER PERFORMANSI

Başlamişli, Ufuk
Yüksek Lisans, Havacilik ve Uzay Mühendisliği Bölümü
Tez Yöneticisi: Prof. Dr. İ. Sinan Akmandor
Şubat 2012, 79 sayfa

Son yıllarda, sınırlı petrol kaynakları, ekonomik ve çevresel nedenlerler, ekonomik açıdan uygun, çevre dostu yakıtlar bulmak amacı ile alternatif yakıtlar üzerinde çok kapsamlı çalışmalar yürütülmektedir. Bu tezde de, alternatif yakıtların motor performansına ve emisyona etkisi deneysel olarak çalışılmıştır. Testler soğuk ve tepkimeli testler olmak üzere iki kısımdan oluşmaktadır. Pompa testlerinde, değişik hızlara göre hacimsel debi ve çıkış basınçları ölçülmüştür. IPI ve PIV tekniği ile enjektörden çıkan yakıtların parçacık çapları, dağılımları, sprey açıları ve iki boyutlu hız dağılımları tespit edilmiştir. Eksoz çıkış sıcaklığı, emisyon ve yanma odası verimi yönünden, alternatif ve JET A-1 yakıtlarının karşılaştırmalı performansları incelenmiştir. Rolls Royce Allison 250 C-18 modeli turbo-şaft motorunda, emisyon, yanma odası çıkış sıcaklık dağılımları, güç türbini giriş ve eksoz çıkış sıcaklıkları, yakıtların motor performansına etkileri detaylı olarak incelenmiş ve parametreler ölçülmüştür.

Anahtar Kelimeler: Alternatif Yakıtlar, Emisyon, Turbo-şaft Motoru,Helikopter Motoru

Dedicated to my family

ACKNOWLEDGEMENTS

I would like to thank my supervisor Prof. Dr. İ. Sinan Akmandor for his guidance support, encouragement and patience throughout the study.

I also would like to thank Mrs. Serap Akmandor, General Manager of Pars Makina Ltd. for understanding and tolerance.

I would like to thank to my colleagues Onur Turan, Serkan Camcıoğlu and research assistant N. Erkin Öcer for their moral and technical support and encouragements.

Special thanks to METU-AE Propulsion Laboratory director Asst. Prof. Dr. Oğuz Uzol and technicians Ahmet Uyar from METU-AE Propulsion Laboratory and Mehmet Özbay from 5. Main Maintenance Center in Ankara and engineers Arif Uçar and Mehmet Karakış from 1. Air Supply and Maintenance Center Command in Eskişehir for tolerances and technical assistances.

The research leading to these results has received funding from the European Union Seventh Framework Programme (FP7/2007-2013) under grant agreement no 211861 (DREAM)

TABLE OF CONTENTS

LIST OF TABLES

TABLES

LIST OF FIGURES

FIGURES

LIST OF SYMBOLS

AFR	Air to fuel ratio
AMD	Arithmetic mean diameter
a	Speed of sound
BE	Bias Error
BTL	Biomass to liquid
CO	Carbon monoxide
CO_2	Carbon dioxide
CTL	Coal to Liquid
d	Particle diameter
f	Fuel to Air Ratio
GTL	Gas to liquid
H_2	Dihydrogen
HRJ	Hydrogenated renewable jet
HVO	Hydrogenated vegetable oil
M	Mach Number
m	Real part of refractive index
$\dot{m}$	Mass flow rate
N	Rotor speed, fringe number, Measurement number
n	Particle number
NO	Nitric oxide
NO_2	Nitrogen dioxide
NO_x	Total nitric oxide and nitrogen dioxide
O_2	Dioxygen
P	Pressure
ppm	Parts per million

PE	Precision Error
SD	Standart Deviation
SFC	Specific fuel consumption
SMD	Sauter mean diameter
SO_2	Sulfur dioxide
T	Temperature
U	Total Uncertainty
UHC	Unburned hydrocarbon
V	Flow speed
XTL	Anything to liquid
x	Measurement value
α	Collecting angle
η	Efficiency
θ	Scattering angle
λ	Wavelength of laser sheet

SUBSCRIPTS

i	Particle number and measurement indices
t	Stagnation properties
b	Burner

SUPERSCRIPTS

-	Mean value

CHAPTER 1

INTRODUCTION

1.1 Literature Survey

In 1999, 2-3 % of anthropogenic carbon dioxide (CO_2) emissions caused from aviation fleet which had 15750 aircrafts in those years [1]. Nowadays this fleet is set to continue to grow and contributes to in greenhouse gas emission by 4.7 % per year. Worldwide aircraft fleet will eventually increase to almost 32000 aircrafts by 2028 [2]. However, the effects on environment is not limited to CO_2, carbon monoxide (CO), total nitric oxide and nitrogen dioxide (NO_x), sulfur dioxide (SO_2), particulate emissions also affect the atmosphere. Beside these environmental concerns supported by international and national regulations, finite petroleum resources, increasing demands and economical issues, make alternative fuels a necessity and offer fuel producers an opportunity [3-4].

Synthetic fuels are alternative fuels that obtained from non-petroleum sources by different processes. One of these processes is Fisher-Tropsch process which is very commonly known in the world. Fisher-Tropsch process was found by two German scientist Franz Fisher and Hans Tropsch in the middle of 1910 and developed in 1923 to reduce the need of Germany for as this is a coal-rich country without any petroleum[5-6]. In this process, feedstock is partially oxidized in the steamed environment by the help of a catalyst to get synthesis gas CO and dihydrogen (H_2) [6]. This synthesis gases are converted to liquid

hydrocarbon again in the presence of a catalyst such as iron and cobalt [7]. Principle chemical equation is given below in Equation (1.1). It is possible to get different hydrocarbon molecules by varying the temperature and pressure at which chemical reaction takes place [5].

$$(2n+1)H_2 + nCO \rightarrow C_nH_{(2n+2)} + nH_2O \quad (1.1)$$

According to feedstock type, different classifications of fuels can be done. GTL, CTL, BTL and XTL refers to gas to liquid, coal to liquid, biomass to liquid and any alternative fuels, respectively. Feedstock are mainly natural gas, coal, biomass and anything respectively. Today's most leading processes are GTL, BTL and CTL [8].

Hydrogenated vegetable oil (HVO) fuels are obtained by hydro-processing of vegetable oils which includes mainly triglyceride. To produce synthetic fuel, feedstock material is deoxygenated. Sulfur, nitrogen and residual material are removed from triglyceride by hydro-treatment and liquid hydrocarbon can be obtained by hydro-cracking and isomerization [9-10]. Another type is Hydro-processed Renewable Jet (HRJ) fuels obtained by hydro-processing of biomass oil [11].

Jet fuels includes several hydrocarbons with a varying carbon number between C_7 to C_{16}. Aviation fuels compose of mainly paraffins and napthenes as 60 % and 25-30 % respectively, less aromatics, alkenes and sulfur, nitrogen and oxygen atoms [12-13]. Synthetic fuels obtained by either Fischer-Tropsch process or hydro-process offers non-sulfur content, non-aromatic content, less nitrogen content. These differences are focused in combustion researches. [3,14]. However, it must be underlined that presence of aromatics has favorable effect on energy content of fuel by increasing the octane number [15]. Furthermore, aromatics results in swelling of o-ring which has good effect on sealing of fuel piping system and prevent the potential shrinkage problems. However, aromatics

have adverse effects on soot formation and smoke [13,16,17]. Synthetic fuels are required to contain at least 8% aromatic contents, because there is no historically leakage problem of conventional kerosene which has no aromatics under this value [18].

Extensive researches on alternative fuels have been conducted in recent years. Sasol, a South African company which has gained approval of semi-synthetic jet fuel for civil aviation in 1999, is carrrying out fully synthetic jet fuel test on very broad range from thermal stability to combustor performance testing. Except the combustor emissions which carried out on Pratt & Whitney JT-9D engine [19], Sasol fully synthetic fuel satisfy the necessary conditions. In terms of CO and NO_x emissions, synthetic fuel have less emissions than conventional jet fuel at all cycles especially 19 % and 4 % in the landing and take-off cycle respectively. In 2009, NASA conducted gaseous and particulate emissions tests on CFM56-2C1 turbofan engine with JP-8 (the military equivalent of JET A-1) and neat Fisher-Tropsch fuels and their blends at different power settings starting with idle to maximum power and at different exhaust measurement locations. As a result, NASA did not detect any major difference in engine performance, as well as NO_x, CO and unburned hydrocarbon (UHC) emissions. Due to nature of synthetic fuels, the SO_2 and particulate emissions are lower from JP-8 to neat synthetic fuels [20]. Another test was carried out at T700 and T701 engine with JP-8 and Fisher-Tropsch fuels in terms of smoke number, particulate and gaseous emissions at three different power settings. These tests showed that Fisher-Tropsch fuels have very small particulate emissions and smoke number with respect to JP-8. However, fuel types have no significant effect on NO_x emission since NO_x emission depends on primarily temperature. Fischer-Tropsch fuels reduced the CO emission as 5-10 % [21]. Shock-Tube Spray experiments and high recirculation combustion rig tests at four different power settings showed that FT fuel and JET A fuels have similar flame stability, NO_x and CO emissions while FT fuel have lower activation energy, less CO_2 emission [3]. Beside the

Fischer-Tropsch fuels, HRJ fuels, their blends and JET A-1have also been tested in Allison Rolls Royce T56-A-15 combustion system [7]. UHC emission is lower for fully synthetic fuels than JET A-1.While NO_x and CO emissions is very similar to JET A-1, CO emission of fully synthetic fuels is lower than JET A-1 as 9-13 %. Some engine manufacturers such as General Electrics, Pratt & Whitney and Rolls Royce conducted engine emission tests with fully synthetic fuels, their blends and conventional jet fuels. While GE measured slight reduction in NO_x emission, increase in CO and UHC emissions, RR and P&W observed no significant difference on emissions [22].

These studies on alternative fuels indicate that alternative fuels generally satisfy the aviation regulations and offer diversity of fuel supply. Although they have improvements in terms of particulate matter, smoke number with respect to conventional jet fuels, they should be further investigated in terms of gaseous emissions. Although fuel manufacturers do not give chemical formulation of fuel, effects of the ratios of paraffins, napthenes, aromatics contents of fuels on combustion and engine performance should be studied in detail [17].

1.2 Objectives

In this study, the main objective is to comparatively measure turbo-shaft engine performance and emission using JET A-1 and alternative fuels. Two alternative fuel are used: GTL and HVO fuels blended with JET A-1 as 50 %. Tests are divided into two sections which are cold tests and reacting tests. Cold tests include the pump performance tests and atmospheric injector tests. The objectives of these tests are to determine the mass flow rate coupled with discharge pressure of fuels with different pump speed, particle droplet diameters and distributions at different fuel nozzle exit pressure by Interferometric Particle Imaging (IPI) method. Reacting flow tests includes the atmospheric combustion

tests, experimental turbojet tests and finally the RR Allison 250 C-18 turbo-shaft engine performance tests. Atmospheric combustion and experimental turbojet tests' purposes are to determine the combustion performance and exhaust gas analysis. Before the final turbo-shaft rig tests, the other tests are designed as preliminary tests to understand and forecast the behavior of alternative fuels and decide whether any modification on turbo-shaft engine controls and hardware is needed or not. Measurement of Combustor exit temperature profile, the overall engine performance figures and exhaust gas emission values at two power settings are constituting the turbo-shaft experiments results.

1.3 Outline

In chapter 2; experimental set-up are introduced and given in details. The measurement conditions and location of tests are described. The main parameters are given in details.

In chapter 3; the measurement results non-dimensionalized with respect to JET A-1 are given and discussed.

In appendix A the procedure of uncertainty analysis is given. In Appendix B, the other similar results of optical velocity measurements are given. In Appendix C, the properties of reference fuel JET A-1 that used in tests are given.

CHAPTER 2

EXPERIMENTAL SETUP AND PROCEDURE

2.1 Pump Performance Test

The pump used during the experiments is power shaft driven rotary gear pump which is currently used on RR Allison 250 C-18 turbo-shaft engine. Pump is a single stage, single element positive displacement pump as depicted in figure 2-1. Pump has a regulator valve, a filter and a filter bypass valve. Fuel enters into pump by inlet port, reaches at low pressure side of gear pump by passing through the filter. Gear pump elements pumps fuel to outlet port with high pressure. It does not need external oil for lubrication, because it is lubricated by fuel re-circulating by high pressure side of gear pump. Regulator valve's mission is to provide boost pressure of secondary filling of gear set, protect against cavitation and prevent fuel vaporization in the pump. Excess bypass flow returns into inlet port. Pressure taps on the pump which are located before filter and after filter are for only monitoring the pressure drop across the filter and maintenance procedure of filter specified by manufacturer. The maximum revolution speed of pump is 3750 rpm.

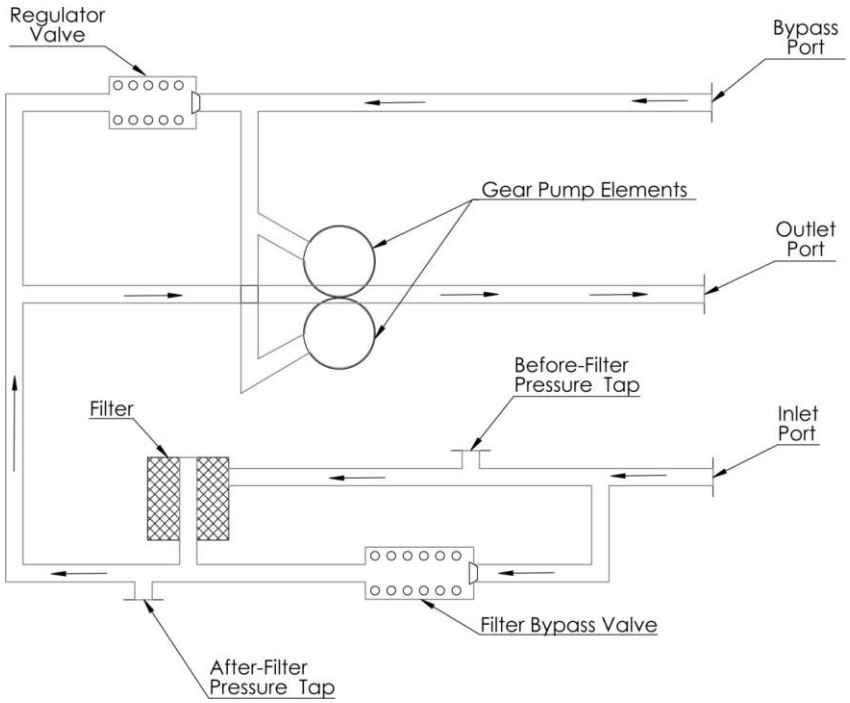

Figure 2-1 Flow Diagram of Pump

Pump experiments are conducted on a separate test rig. Here the pump is externally driven by Simovert controlled 200 kW electrical motor in METU AE Propulsion Laboratory. They are connected by a shaft manufactured according to pump technical specifications. RPM can be adjusted by input voltage of electrical motor. The inlet port of rotary gear pump is pressurized by a first small fuel pump to 1 atm pressure gage due to its working principle of RR Allison 250 C-18 engine. There exists an original nozzle at the outlet of rotary gear pump. Pressurized fuel returns to a different fuel tank, to prevent the heated fuel to return to the initial tank and affects the measurements.

Measured parameters are pump inlet temperature, pressure, outlet pressure, temperature, mass flow rate and torque. Temperatures are measured by J-types thermocouples which have very common usage for lower temperature scale especially 0-300 °C. Pressures are measured by very high sensitive Ku-lite pressure transducer. Torque on shaft is measured by rotary torque-meter which placed between electrical motor and gear pump. Fuel flow rate is measured by a

volumetric fuel flow measurement device. Except inlet pressure which is only for monitoring, all parameters are recorded by data acquisition system as depicted in figure 2-2.

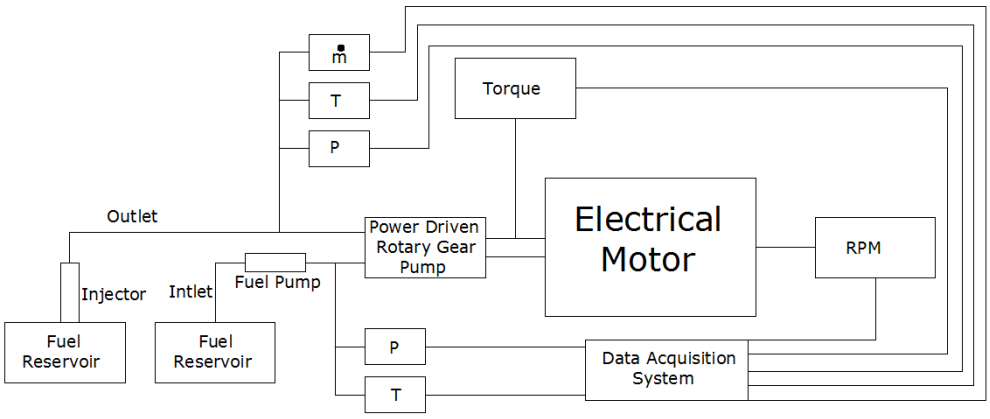

Figure 2-2 Pump Test Setup

Pump experiments are conducted for different pump speed starting from 750 rpm to 3750 rpm.

2.2 Combustor Injector Spray Test

The aim of this experiment is to determine droplets characteristics in terms of arithmetic mean diameters (AMD) and sauter mean diameters (SMD), spray cone angle and 2-D velocity distributions of conventional fuel JET A-1 and alternative fuels GTL blend and HVO blend. Droplets diameters are calculated by IPI technique and 2-D velocity distribution is calculated by particle imaging velocimetry (PIV) technique.

The theory behind the IPI technique is scattering theory. Process of this technique can be summarized that as reflected and refracted rays through the spherical and

transparent fuel droplets forms two glare point on focal plane. These two glare points coincide and result in fringe pattern on de-focal plane. Fringe numbers is directly related with particle diameter.

$$d = \frac{2\lambda N}{\alpha} \frac{1}{\cos(\theta/2) + \frac{m \sin(\theta/2)}{\sqrt{m^2 - 2m\cos(\theta/2) - 1}}} \quad (2.1)$$

λ is the wavelength of the laser sheet, m is the real part of the refractive index of fluid, θ and α is scattering and collecting angle respectively. Only input coming from fluid side is refractive index and it is internal property. Refractive index measurements of conventional and alternative fuels were performed by METU Petroleum Research Center. Refractive index measurements results are shown in Table 2-2.

Table 2-1 Refractive Index Results

FUEL TYPE	METHOD	REPETABILITY	REFRACTIVE INDEX
JET A-1	ASTM D 1218	0.0002	1.4408
GTL BLEND			1.4330
HVO BLEND			1.4337

Figure 2-3 shows the combustor injector spray test setup. Setup consists of Nd:Yag laser which generates a wavelength of 532 nm with a maximum 200 mj/pulse a repetition of 15 Hz, 2 CCD camera with 12 bit grayscale within a spatial resolution 1344 x 1024 pixels, a synchronization unit, fuel nozzle of helicopter turbo-shaft engine, adjustable holder which can provide changing measurement window fuel to dissipate outside measurement domain, is provided by small radial fan. More specifically, the aim of sheet air flow is to protect the beam splitter surface from fuel droplets vapor. The fuel nozzle has very condensed spray pattern and the cameras should be relatively closer than PIV for

IPI measurement. Therefore, a protection is necessary to sustain healthy measurement without intervention in fluid flow.

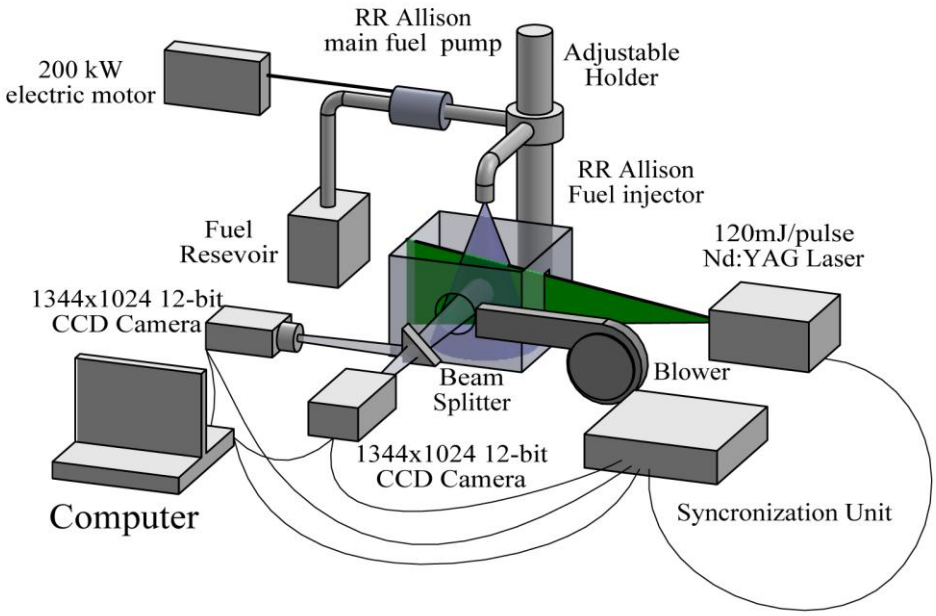

Figure 2-3 Combustor Injector Spray Test Setup

During this experiment, scattering angle θ is set as 80° and collecting angle α is set as 14°. Figure 2-4 displays position of cameras relative to spray.

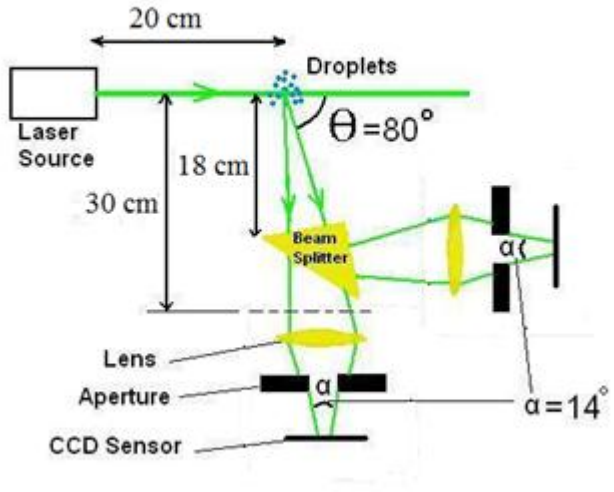

Figure 2-4 Position of Cameras and Laser Source

Focal camera is just only for velocity measurement while de-focal camera is needed for both velocity and particle sizing. In other words, IPI needs only de-focal camera but PIV measurements requires both cameras. The position of particle should be validated by both camera to obtain measurement accurately. For IPI data acquisition and evaluation, a calibration which ensure overlap between the focused and defocused images, should be performed. Calibration is done by taking the image of target plane by both cameras and calculating the mapping points on the image plane by applying Imaging Model Fit method. These images have a resolution of 1344×1024 pixels. Target plane as depicted in Figure 2-5, is 200×200 mm wide, has 5 mm spacing between dots. Zero marker diameter is 2.7 mm, main marker is 2.0 mm and axis marker is 13 mm.

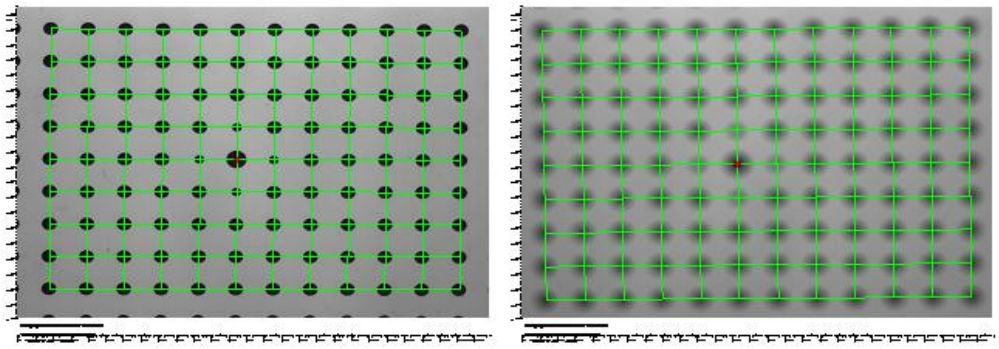

Figure 2-5 Target Plane and Image Model Fits for Calibration

Figure 2-6 and 2-7 show the raw image and processed image taken from de-focal camera respectively. 5×5 Laplacian filter is applied to raw image to reduce noise level. Laplacian filter is a high pass filter which retains high frequency information while reducing the low frequency information to improve fringe pattern.

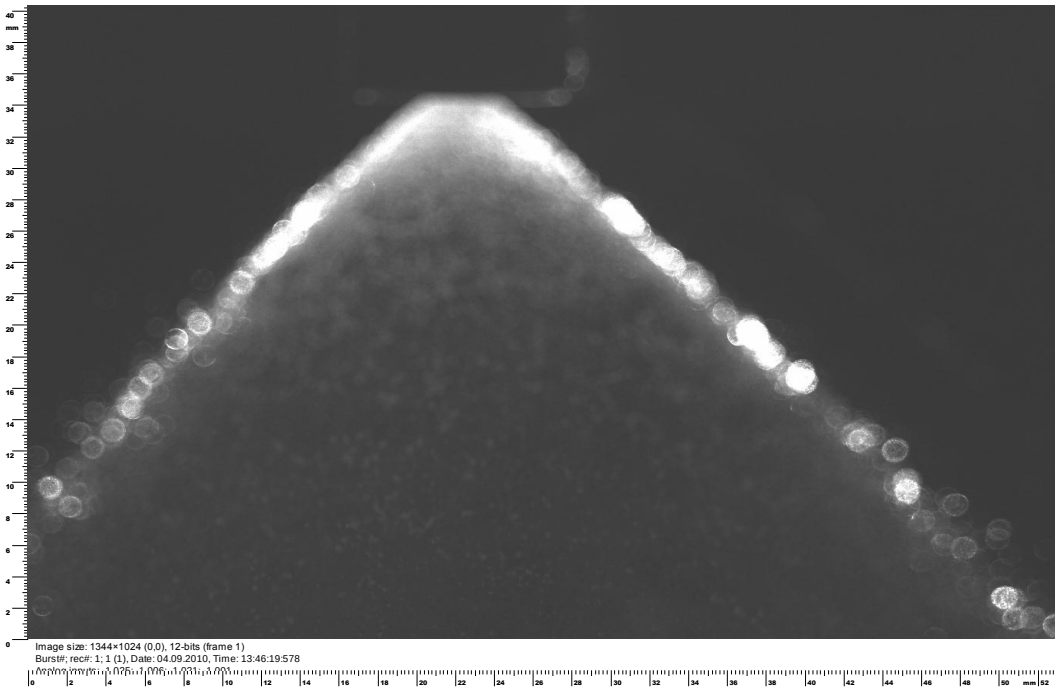

Figure 2-6 Raw Image

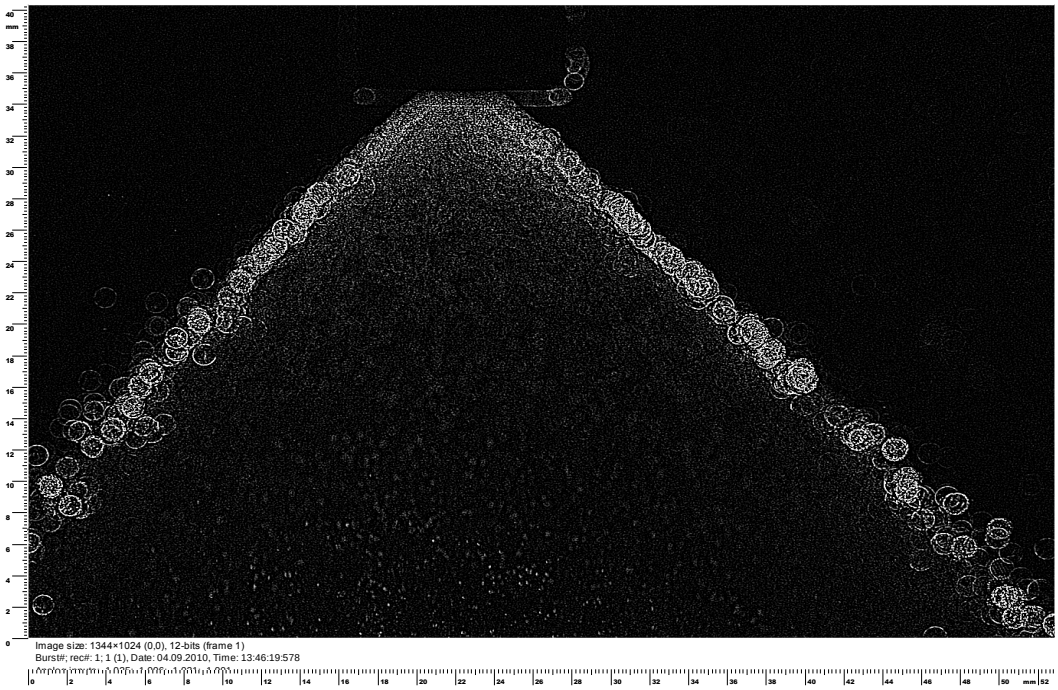

Figure 2-7 Processed Image

Main droplets occur at sides of flow due to hollow cone fuel injector. Therefore, the filtered image is masked as depicted in figure 2-8, to focus on mainstream of flow, reduce noise level caused from fluid vapor returning from tank, reduce computational time, assuming axisymmetric flow.

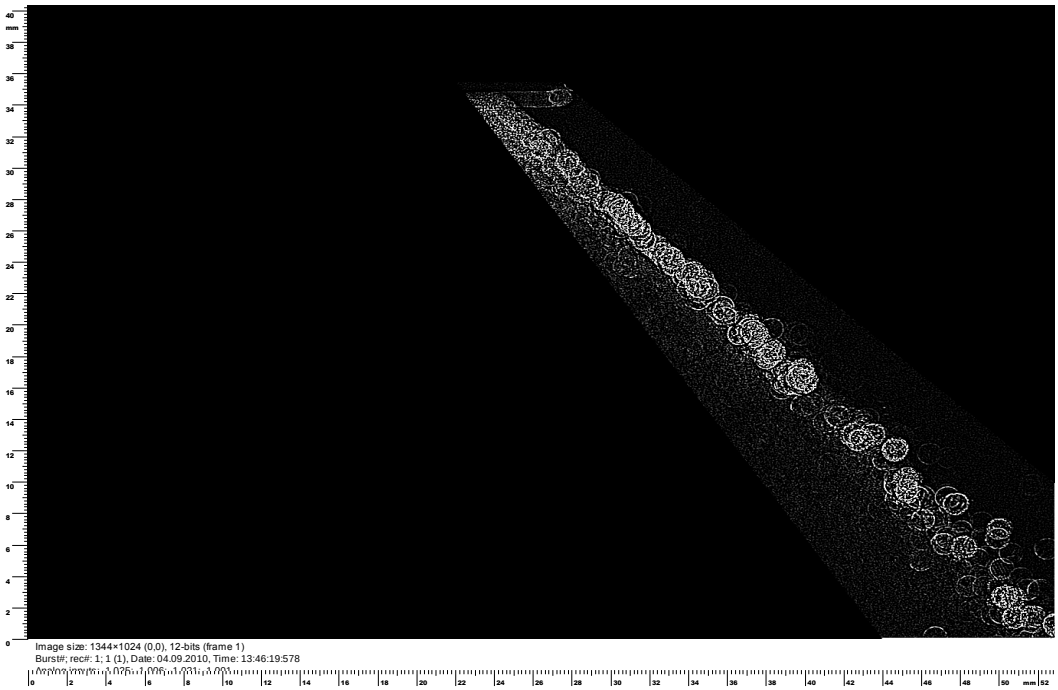

Figure 2-8 Masked Image

Figure 2-9 shows the droplet calculation from one masked image. Red particles imply not validated particle but green particles are validated particles by both focused and de-focused camera. To increase particle validation, number of taken images should be increase. Current camera setting is not enough to measure and validate particle droplets due to very condensed flow at the exit of fuel nozzle, hence validated particles increase away from the fuel nozzle exit.

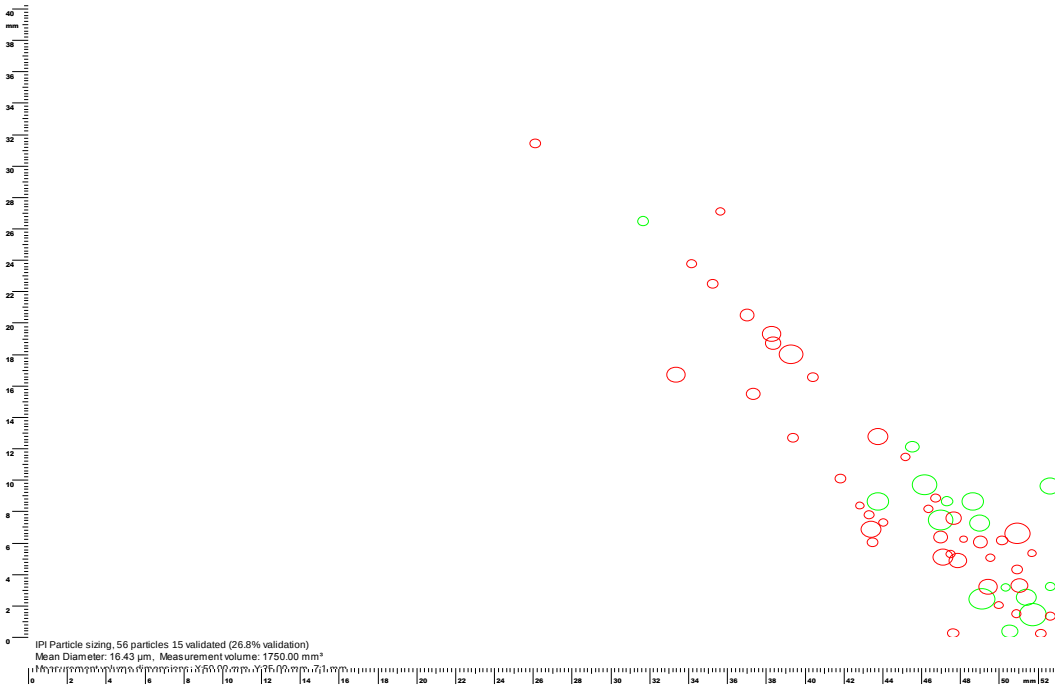

Figure 2-9 Droplet Calculation

Two measurement window configuration are selected. Window dimensions are 40 × 50 mm. Both window are masked for mainstream flow. Intersection area of two window is 10 × 15 mm. A taken image is shown in figure 2-10.

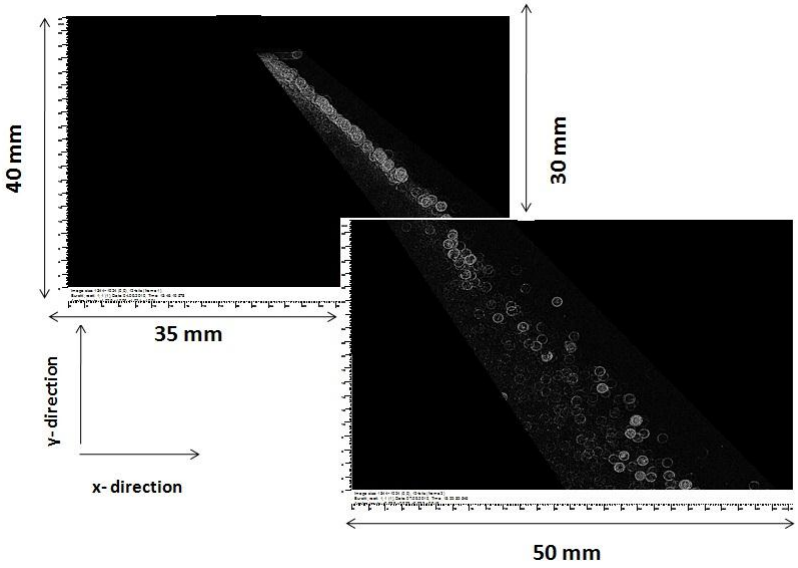

Figure 2-10 Measurement Window Configuration

AMD is division of summation of total particle diameter multiplied with corresponding particle number, to total particle number.

$$AMD = \frac{\sum_i^N d_i\, n_i}{\sum_i^N n_i} \tag{2.2}$$

SMD is surface area moment mean which is very common usage in combustion and is calculated as

$$SMD = \frac{\sqrt[3]{\sum_i^N d_i^3\, n_i^3}}{\sqrt{\sum_i^N d_i^2\, n_i^2}} \tag{2.3}$$

Small disturbances in flow may result in wrong angle calculation. Therefore, cone angle measurement is performed by taking mean pixel average value of raw images to eliminate these disturbances. Mean pixel average image of thousand raw images is displayed in figure 2-11.

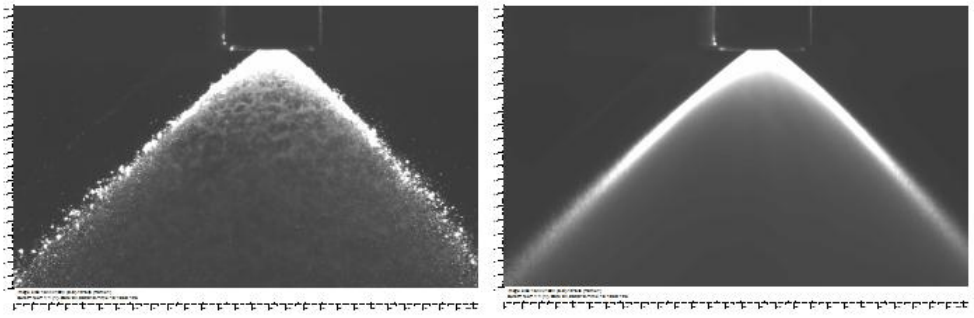

Figure 2-11 Raw and Mean Pixel Averaged Images

Experiments are performed at four different fuel nozzle pressure. For each pressure setting, experiments are repeated seven times to validate the

repeatability. Thousand images are taken and analyzed for both IPI and PIV measurement at each pressure setting.

2.3 Atmospheric Combustion Tests

Atmospheric combustion tests are performed at C 491 combustion unit manufactured by PA. Hilton Ltd in METU AE Propulsion Laboratory. Figure 2-12 shows the experimental set-up. Combustion unit had been designed for both gas fuel and liquid fuel combustion.Gas fuel combustion process is first launched, after a warm-up liquid fuel is injected together with gas fuel combustion, finally liquid fuel combustion goes on after shutting down gas fuel. Combustion unit is controlled by manual valves. It has blower to take air almost near the atmospheric pressure inside combustion unit. During the experiments, air is set as maximum, cooling water is set as constant. The liquid fuel is only control parameter changing the flow rate.

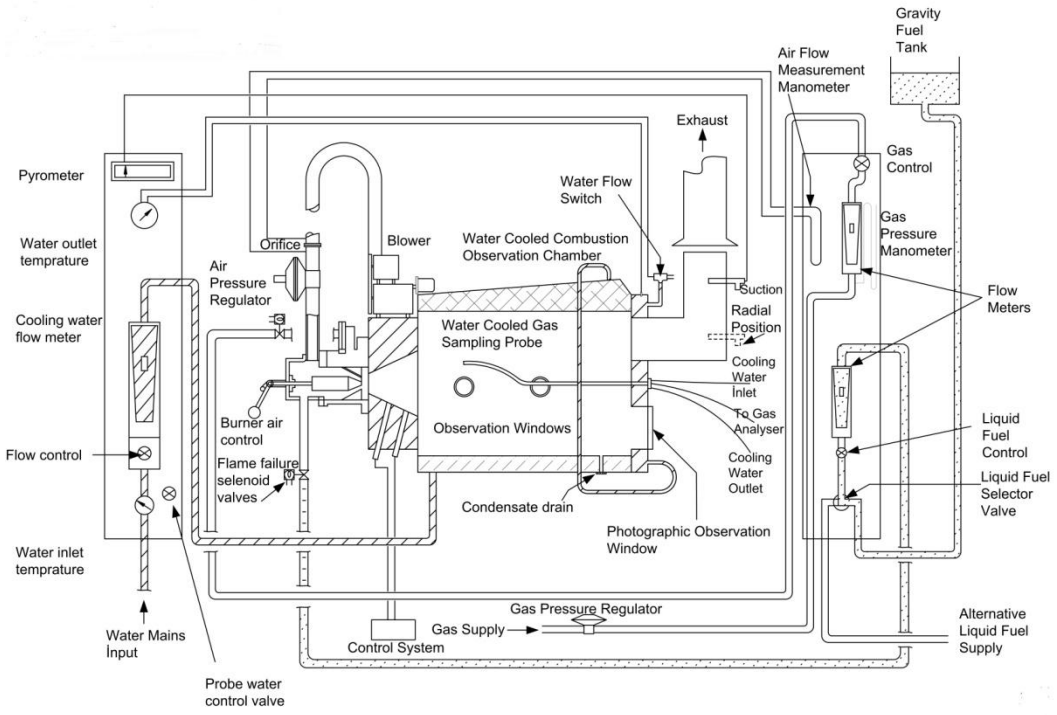

Figure 2-12 Atmospheric Combustion Test Setup

Measurement parameters are exhaust gas temperature and emissions. Temperature measurements are performed by K-type grounded thermocouples which has very common usage in high temperature measurement. Emission measurements are conducted by TESTO 350 gas analyzer (Figure 2-13). Current configuration of gas analyzer provides the O_2 and CO_2 as volumetric, NO, NO_2, total NO_X, SO_2 and H_2 as parts per million (ppm). For an accurate measurement, gas analyzer measurement need a minimumdata acquisition time specified by manufacturer for each emission type. Reaction times changes between 20 second and 1 minute, all experiments are performed with 5 minutes data acquisition time so as amply satisfy the necessary reaction time.

Figure 2-13 TESTO 350 Gas Analyzer

The input parameter is Air to Fuel Ratio (AFR). Four different AFRs which varies between 19.9 to 31.8 are selected.

2.4 Experimental Turbojet Test

The aim of this facility is to determine the burner efficiency, specific thrust and specific fuel consumption (SFC) of different fuel on turbocharger based turbojet engine.

Experimental turbojet engine has a capacity of 0.2 kg/s intake air mass flow. Maximum operating speed is ≈ 100.000 rpm and nominal compression ratio 1:2.

Experimental Turbojet Engine Set-up had been developed from a diesel engine turbocharger. Turbocharger has one stage centrifugal compressor and centrifugal turbine coupled with a single and simple shaft. A can type combustion chamber, which has two main components the casing and the liner, had been designed and

manufactured by Inconel 718 material, only swirl cup was made of Hastelloy X. A propelling nozzle had been designed and manufactured iron jet pipe with a stainless steel central plug used for changing the exit area. The engine inlet consists of two parts. Inlet pipe servers the purpose of providing fully developed, completely axial flow into compressor as starter and after certain rpm which engine can sustain itself, it is taken. Aft inlet is displaced in front of turbocharger compressor. The experimental turbojet engine has two adapter parts which are compressor-burner adapter and burner-turbine adapter. Compressor-burner adapter guides the flow from compressor volute to the combustion chamber. It is compromised of the adapter pipe and 180° turning duct. Burner-turbine adapter leads the hot gasses from the combustion chamber to the inlet of the turbine volute. Atomization of fuel is provided by oil burner spray nozzle and operates between 1-15 bar. The auxiliary system consists of lubrication, ignition and fuel system. A detailed information about experimental turbojet is given in [23].

Except gas fuel control, other system has been controlled by computer based control system. LPG has been used manually in a very small time to start and warm up engine, ignition of liquid fuel. While, open-close of electrical valve of liquid spray injector and liquid fuel pump are controlled by computer, the mass flow of liquid fuel is adjusted by manual valve. Lubrication system in the experimental turbojet engine feeds the two roller bearings of the turbocharger with pressurized lubrication oil. The cooling system is a re-circulating type and requires external three phase electricity supply. Ignition system has a spark plug and ignition unit and fed by 12 V DC power supply. Fuel system divides into two which are liquid and gas fuel system. The experimental turbojet set-up is given in figure 2-14.

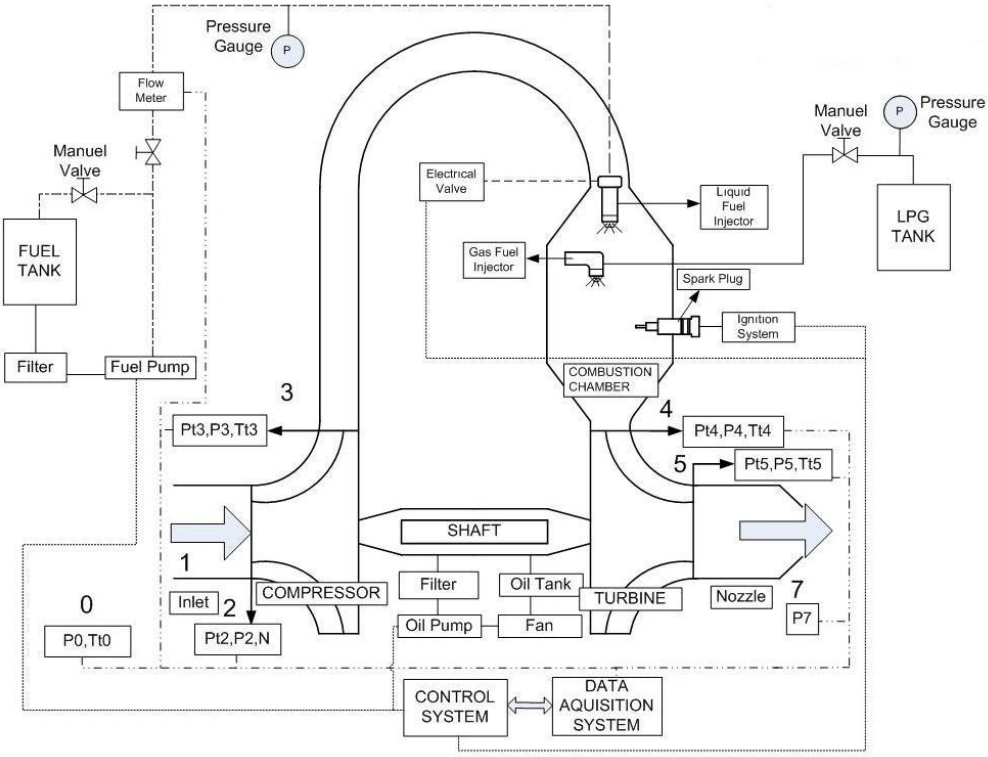

Figure 2-14 Experimental Turbojet Test Setup

Taken measurements from experimental turbojet engine are atmospheric total pressure and temperature (P_{t0}, T_{t0}), compressor inlet total and static pressure (P_{t2}, P_2), rotor speed N, compressor exit total and static pressure and total temperature (P_{t3}, P_3, T_{t3}), turbine inlet total and static pressure and total temperature (P_{t4}, P_4, T_{t4}), turbine exit total and static pressure and total temperature (P_{t5}, P_5, T_{t5}), nozzle exit static pressure P_7 and fuel mass flow and observed parameter are oil pressure, temperature and liquid fuel pressure just before fuel nozzle. Assumption made are that T_{t2} is equal to T_{t0} due to very small duct length, negligible temperature variation, T_{t5} is equal to nozzle exit total temperature (T_{t7}) due to very small duct length, negligible temperature variation and finally P_{t5} is equal to nozzle exit total pressure (P_{t7}) due to very small duct length, negligible pressure variation.

Run procedure is that initially engine is started with another air supplier via inlet pipe. Then gas fuel is given and burnt. At less than 30000 rpm, liquid fuel is given and burnt by gas fuel. After less than one minutes of run time, gas fuel is closed and engine runs with only liquid fuel. Combustion chamber casing is externally cooled on the outside due to very high temperature and turbojet engine can sustain itself after 30000 rpm by intake air compressed through the radial compressor. The speed of engine is adjusted by manual valve of liquid fuel line and measurements are taken at different rotor speed.

2.5 RR Allison 250 C-18 Turbo-shaft Engine Test

The turbo-shaft engine tests are performed on RR Allison C-18 turbo-shaft engine located in METU-AE Propulsion Laboratory. As depicted in figure 2-15, RR Allison 250 C-18 turbo-shaft engine is reverse flow combustion engine. Take-off power is 236 kW and maximum continuous power is 200 kW. Compressor section consists of 6 stage axial and one last centrifugal stage. The compressed air is discharged into two external ducts which guide the air flow into combustion chamber. Maximum compression ratio is 1:6 and maximum air intake is 1.3 kg/s. Outer combustion case and combustion liner forms the combustion chamber. A spark ignitor and fuel nozzle are located at the aft end of outer combustion case. Compressed air from the compressor enters into combustion liner through the holes in the liner dome and skin. Compressed air is mixed with fuel spray and results in combustion with ignition. Turbine section consists of two gas producer (high pressure) turbine stage and two free power (low pressure) turbine stage. Gas producer turbines drive the compressor section and accessories gear train in the gearbox bottom of engine. Maximum speed of gas producer turbine is 51120 rpm. Free power turbine drives the main rotor of helicopter by reduced speed through the gearbox. Its maximum speed is 35000

rpm. Power output shaft maximum speed is 6000 rpm. The expanded gas through the turbines is discharged by the V-type twin ducts in the upward direction. Gas producer turbine speed is named as N1, free power turbine speed is named as N2 and power output shaft as N3.

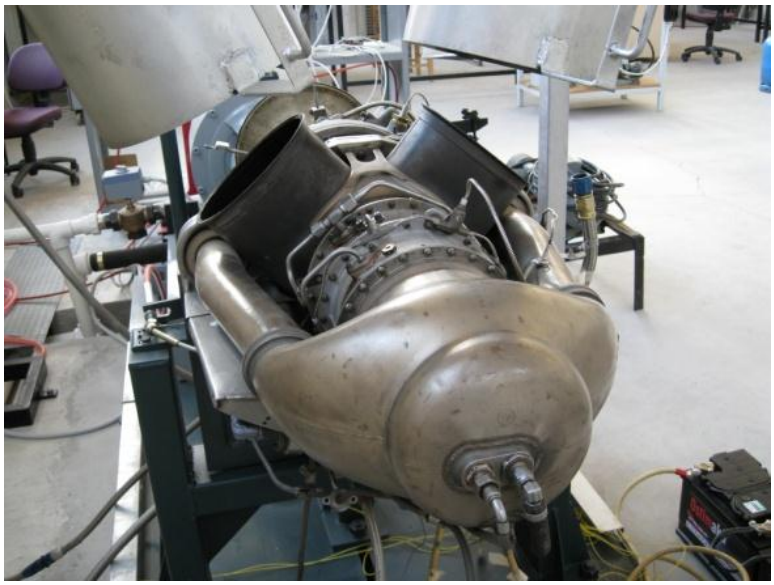

Figure 2-15 RR Allison 250 C-18 Turbo-shaft Engine

Turbo-shaft test setup is shown in figure 2-16. Power output shaft is connected to water brake dynamometer. Engine is loaded with dynamometer instead of helicopter main rotors on ground tests. Run procedure: starter motor drives the gas generator turbines. At 15 % of N1 speed, governer is taken to ground-idle position. During the start-up, the operator should be ensured that power turbine inlet temperature, oil pressure and oil are in the limit. For loading process, N1 and N2 speed should be 100 % of their speed.

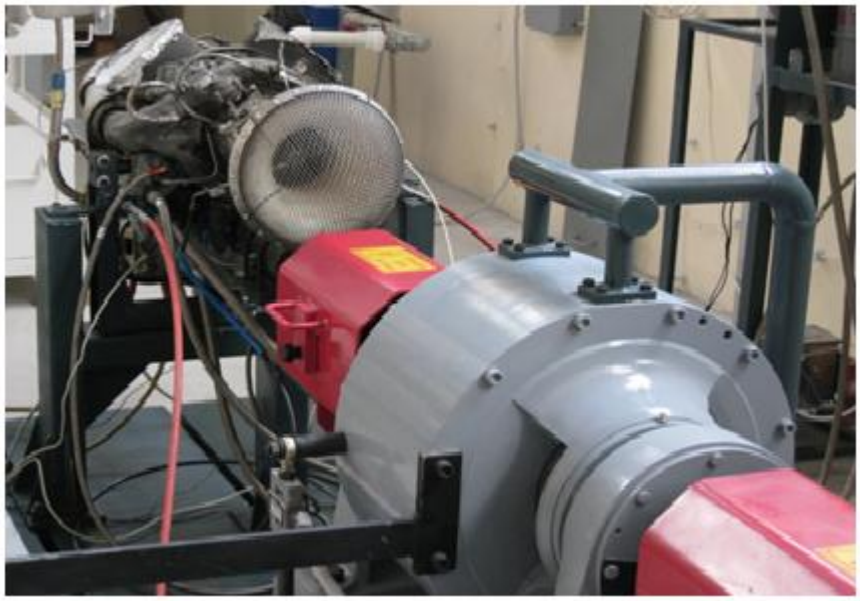

Figure 2-16 RR Allison 250 C-18 Turbo-shaft Engine Test Setup

RR Allison 250 C-18 turbo-shaft test setup and measured parameters are shown in figure 2-17. Torque, dynamometer water inlet and exit temperature and pressure are measured from dynamometer. N1, N2 and N3 speed with other engine parameters are measured from turbo-shaft engine. N3 speed and torque are used for engine power calculation. Exhaust gas content is measured at exhaust duct by TESTO 350 gas analyzer previously used for atmospheric combustion test. Gearbox parameters are measured only for monitoring to ensure a safe engine operation.

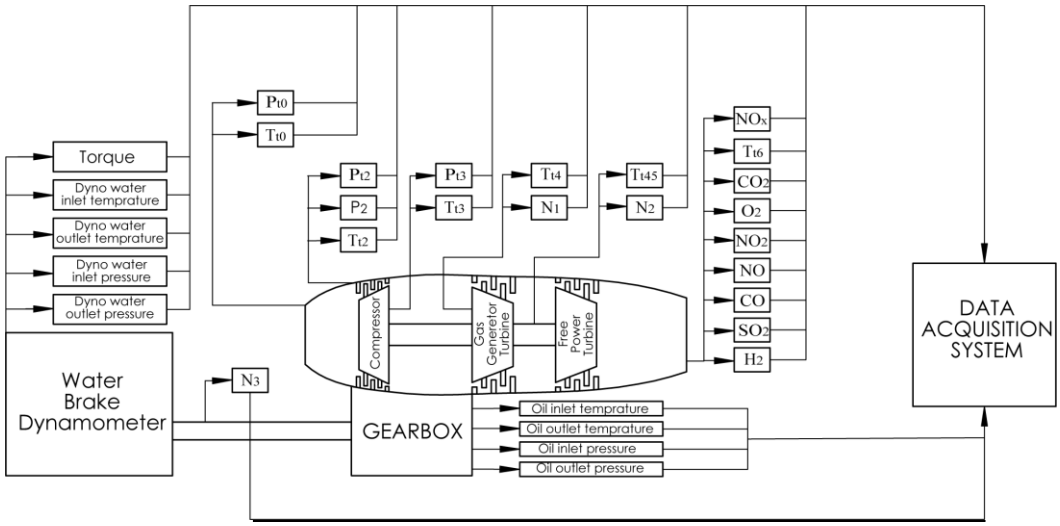

Figure 2-17 RR Allison 250 C-18 Turbo-shaft Engine Test Setup and Measurement

In addition to these measurements, radial temperature distribution is measured at the exit of combustion chamber. The location of thermocouples is displayed in figure 2-18. Combusted flue gas radial temperature profiles are measured at three circumferential positions. Combustion chamber has 155 mm outer diameter measured at high pressure turbine inlet. Starting from outer most combustion liner radii, the temperature within combustor at exit condition are measured radially inward 1 cm interval to adequately cover turbine inlet annulus. At lower radial locations closer to engine centerline, the interval between measured locations increases to nearly 2 cm. In overall, temperature is measured at 10 radial points fat three tangential position at turbine inlet. K-type thermocouples are used for radial distribution measurement. Inconel protecting tubes for thermocouples are used due to high temperature gas coming from combustion chamber. Because thermal loads on turbine are very high, extreme care has been taken as any particle accidentally detaching from thermocouples may damage the turbine blades.

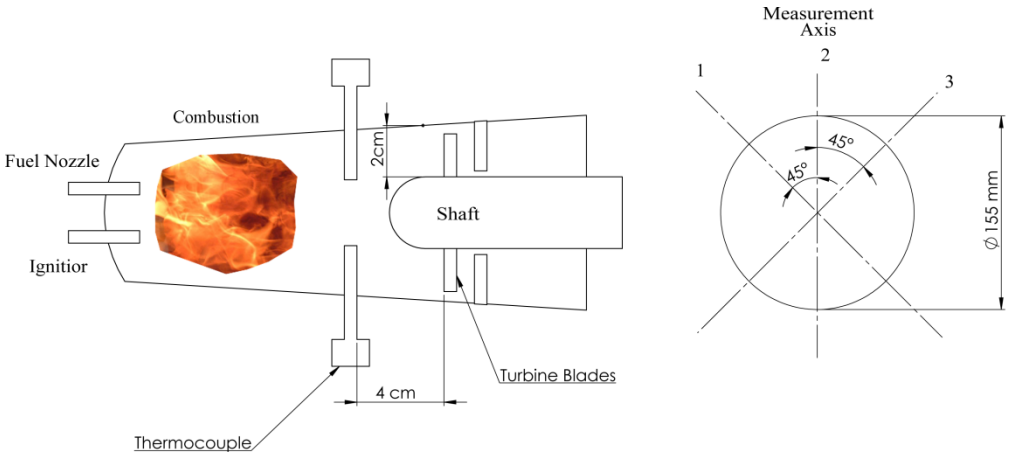

Figure 2-18 Radial Temperature Measurement At The Exit of Combustion Chamber

Tests are performed at three engine run settings. These are ground-idle start-up, ground-idle stop which are almost same power as 20 kW and cruise 100 kW power settings. Tests are carried out 15 times for each fuels to validate the measurement results repeatability.

CHAPTER 3

EXPERIMENTAL RESULTS

3.1 Results of Pump Performance Test

Fuel mass flow rate, discharge pressure, discharge temperature and torque for different pump speed were measured for reference fuel JET A-1 and two alternative fuels, namely a GTL blend and HVO blend. Pump inlet temperature for reference and alternative fuels is 20 °C. The results are non-dimensionalized with respect to JET A-1 value at lowest pump speed value.

There are no major differences between alternative fuels and reference fuel in terms of discharge pressure and volume flow rate as depicted as figure 3-1 and figure 3-2 respectively. Pump is choked after pump reaches speed around 1494 rpm. HVO blend reaches a slightly lower pressure plateau and the corresponding flow rate at high rpm's is correspondingly lower until 3250 rpm shaft speeds. HVO blend exhibits slightly higher stability in pumped output flow rates. GTL blend provides lower flow rates at corresponding low shaft speeds, proportional to gradually increasing flow rate until 1494 rpm. At high speeds exceeding 2250 rpm, GTL blend fuel pumping performance is recovered and exhibits a higher flow rate and higher pressure output as well. Total uncertainty in discharge pressure is ± 35 kpag and ± 0.08 lt/min for fuel volume flow rate for all fuel.

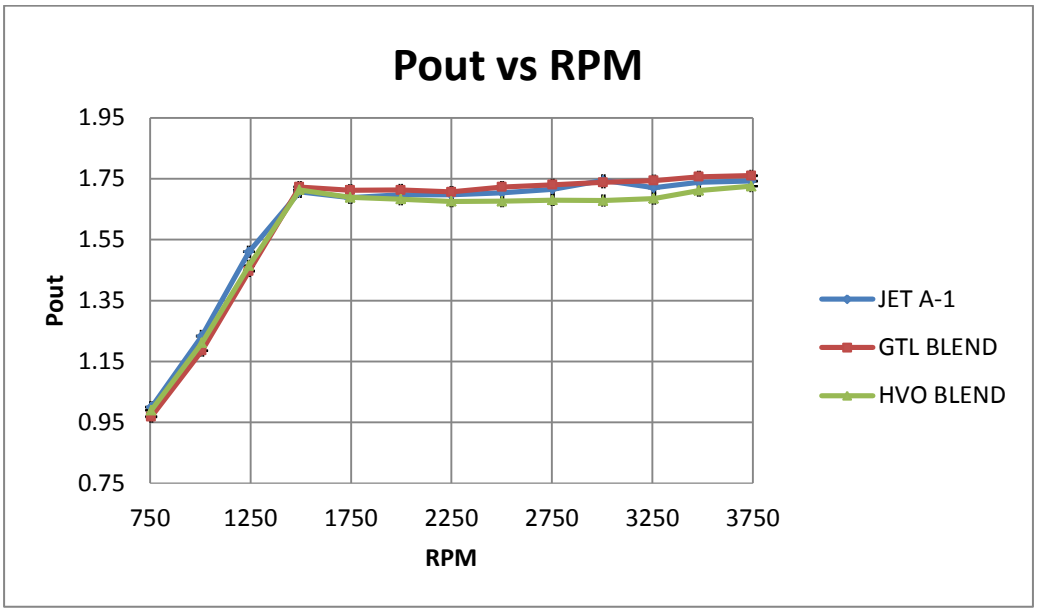

Figure 3-1 Discharge Pressure vs. Pump Speed

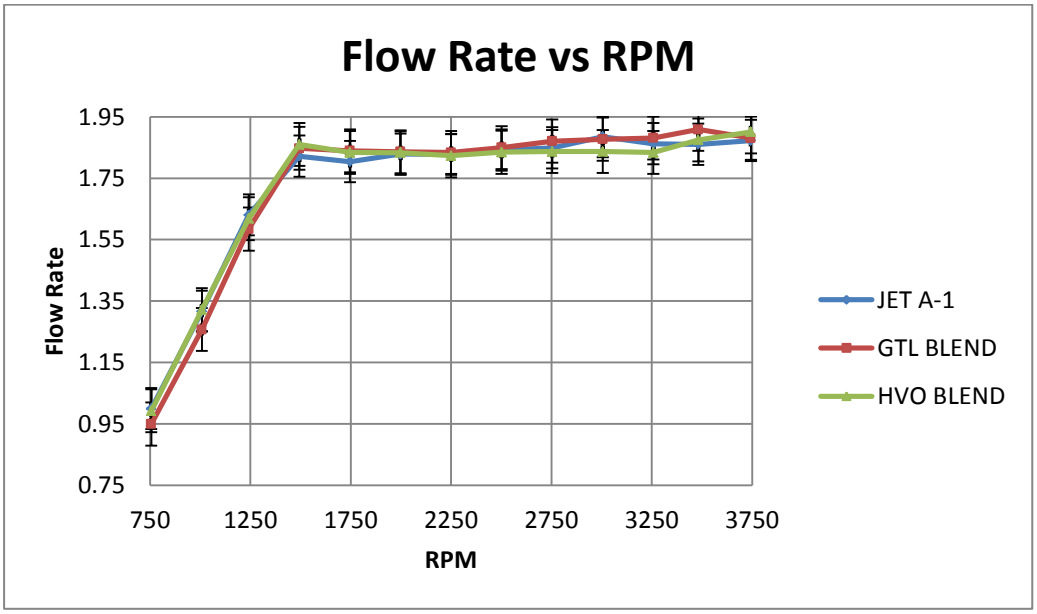

Figure 3-2 Fuel Flow Rate vs. Pump Speed

The discharge temperature of alternative fuels is higher as around 2 °C than conventional jet fuel as depicted in figure 3-3. In discharge temperature

measurements, total uncertainty is ± 0.2 °C for both alternative fuels and ±1.1°C for reference Jet A-1 fuel.

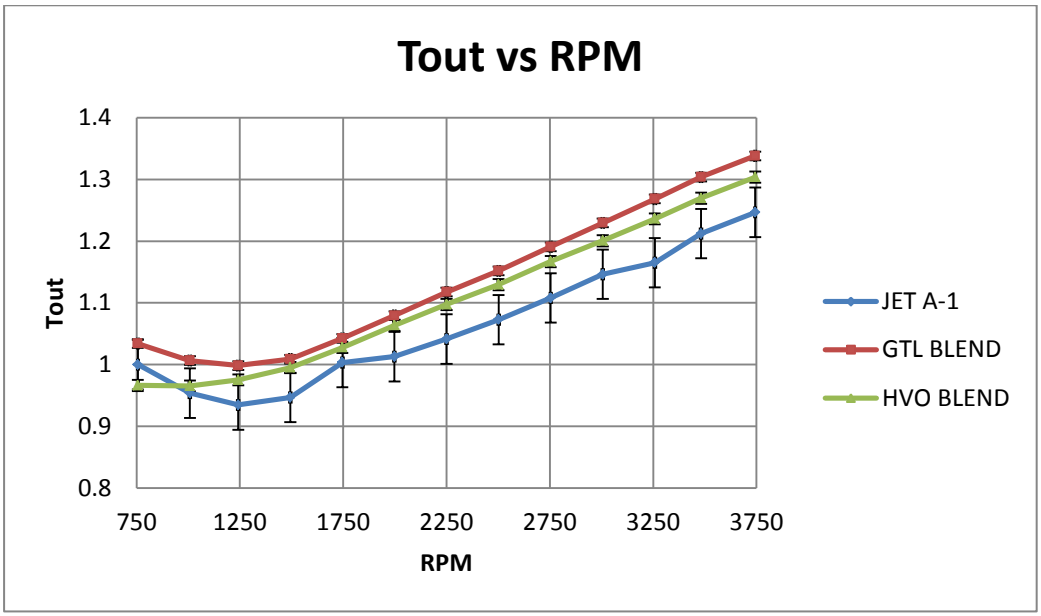

Figure 3-3 Discharge Temperature vs. Pump Speed

Torques plotted against to pump speed is shown in figure 3-4. All fuels have same torque distribution until 2000 rpm, but after this speed, torque of JET A-1 fuel is greater than pump torque using alternative fuels by 0.2 Nm. Since pumped mass flow rate and pressure is almost the same, lower pump torque for alternative fuels correspond to a saving in input pump shaft power. Total uncertainty in torque measurement is ± 0.1 Nm.

As a conclusion, there is no major difference between alternative fuels and conventional fuel in terms of pump characteristics. These results were expected because alternative fuels had been subjected to same standards as JET A-1 in terms of viscosity and density.

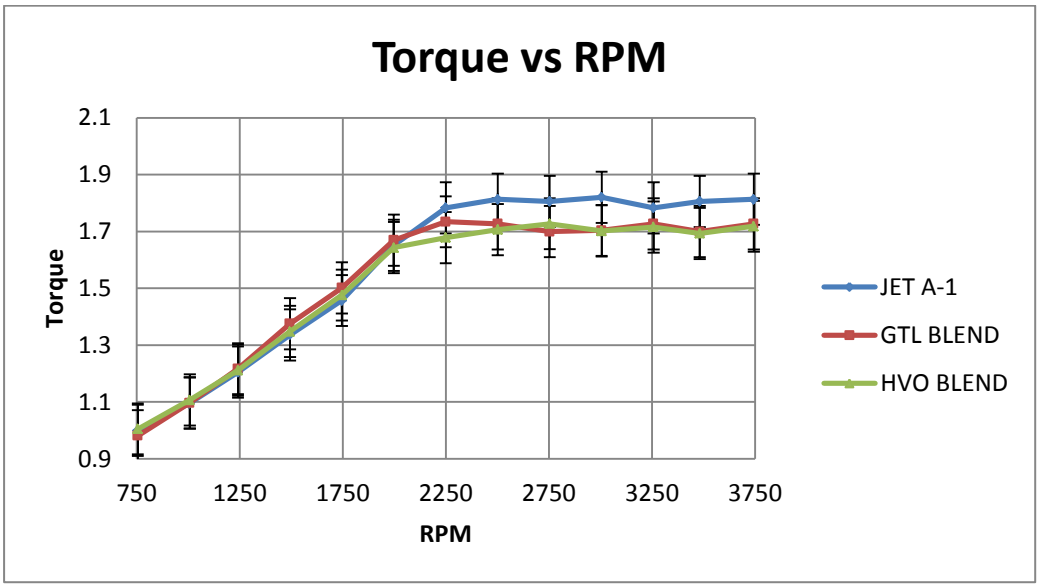

Figure 3-4 Torque vs. Pump Speed

3.2 Results of Combustor Injector Spray Test

Droplet size distribution, cone angle and 2-D velocity distributions were measured for reference fuel JET A-1 and alternative fuels GTL blend and HVO blend using IPI and PIV methods. Nozzle discharge temperature is around 30° C during spray tests. Measurement results are normalized with respect to JET A-1 AMD value at lowest nozzle discharge pressure at 1st window.

In AMD,SMD and cone angle measurements, error bars show the precision error. Theoretically, the determination of instrumental error is difficult. Because, the error in vertical orientation and thickness of laser sheet, wavelength of laser source, aperture size of cameras and scattering angle should be known exactly. However, it is important that figures show the trend of distribution in AMD, SMD and cone angles of fuels. The main reason of trend cannot be exactly determined without knowing of fuel nozzle working principle and geometry.

All fuels have similar trend for both measurement window as depicted in figure 3-5 and figure 3-6. From 1st window to 2nd window, particles tend to combine which results in greater droplet diameters. Alternative fuels and JET A-1 have very similar behavior for 1st, but they reach the same value at higher pressure for 2nd window. Maximum difference between alternative fuels and JET A-1 is approximately 2 µm. Furthermore, GTL blend and JET A-1 droplet diameters change as 1 µm during the fuel nozzle pressure variation, variation in diameter for HVO blend is 2 µm. In other words, HVO blend fuel atomization is less uniform. Precision error of GTL blend and JET A-1 are 0.05 µm and 0.08 µm respectively, while it is 1 µm for HVO blend.

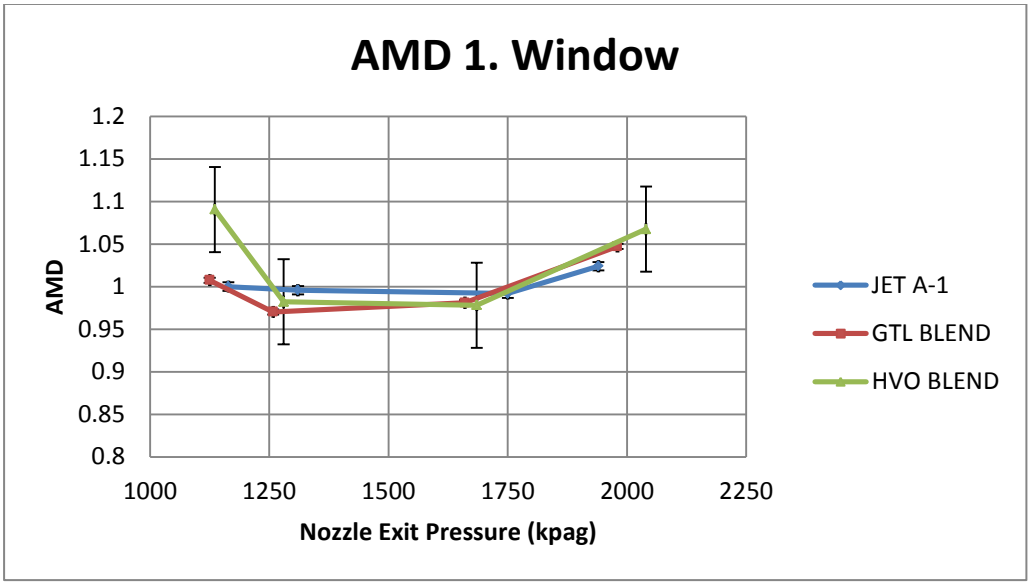

Figure 3-5 Arithmetic Mean Diameter vs. Fuel Nozzle Exit Pressure 1st Window

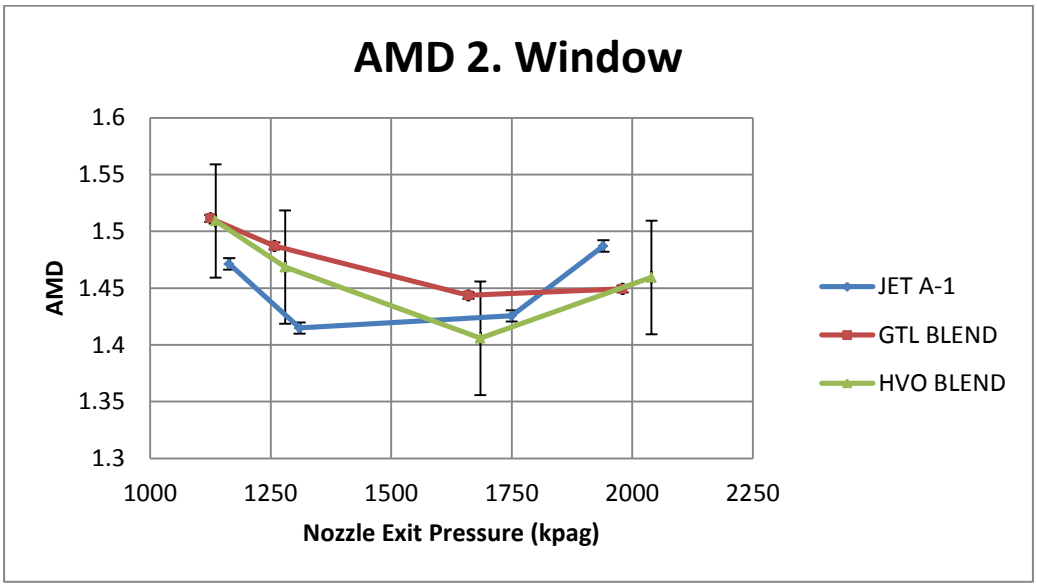

Figure 3-6 Arithmetic Mean Diameter vs. Fuel Nozzle Exit Pressure 2nd Window

All fuels have similar trend for 1st but this trend is not observed for 2nd window for HVO blend in terms of SMD (Figure 3-7 and Figure 3-8). For 1st measurement window, GTL blend and JET A-1 has very closer SMD while HVO blend differs by as much as 1 µm. GTL blend tends to decrease continuously, while SMDs of HVO blend and JET A-1 starts to increase after fuel nozzle discharge pressure 1750 kpag for 2nd measurement window. GTL blend and JET A-1 precision errors are 0.12 µm and 0.2 µm respectively and 1.3 µm for HVO Blend.

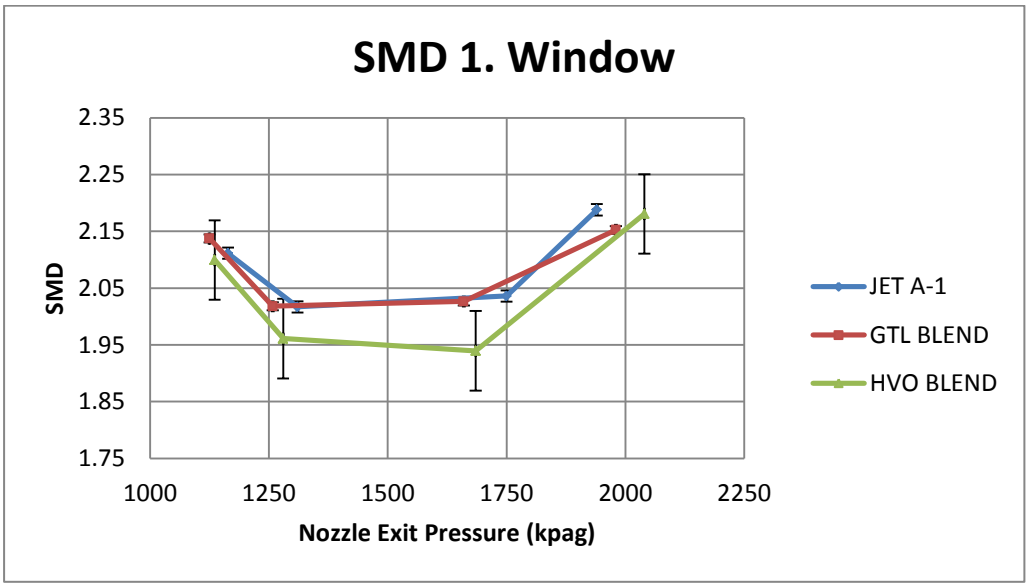

Figure 3-7 Sauter Mean Diameter vs. Fuel Nozzle Exit Pressure 1st Window

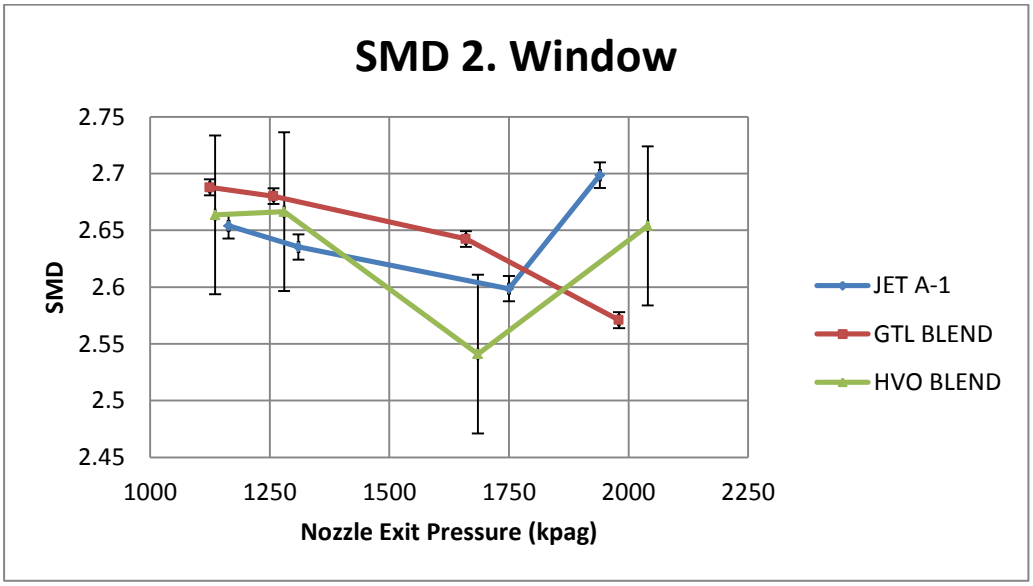

Figure 3-8 Sauter Mean Diameter vs. Fuel Nozzle Exit Pressure 2nd Window

Figure 3-9, 3-10, 3-11, 3-12 give the arithmetic droplet distribution for lowest and highest fuel nozzle exit pressure corresponding to 1125 and 2000 kpag. All fuels have two peak values which are approximately 7 µm and 17 µm for 1st window and 8 µm and 21 µm for 2nd window. Beside this, the effect of higher

peak value increases on the mean droplet diameter estimation for 2nd window because the particles tend to coalesce and validated particle increases from 1st to 2nd window as well. Figures also show that total droplet numbers for GTL blend and JET A-1 captured and validated by the cameras are higher than HVO blend. Only different input parameter is refractive index during experiments. This may affect the droplet distribution.

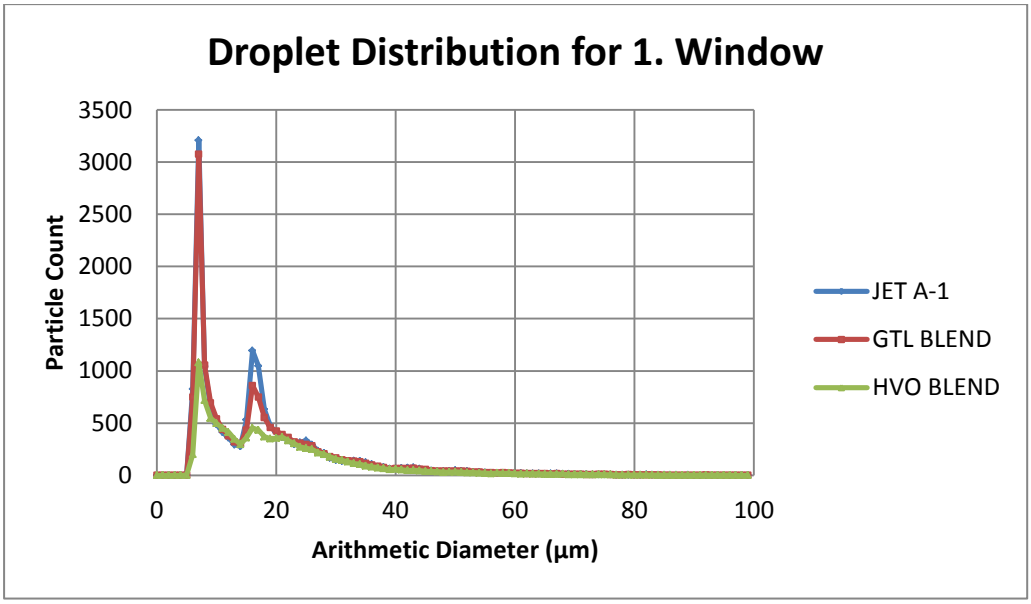

Figure 3-9 Arithmetic Droplet Distribution at 1125 kpag for 1st Window

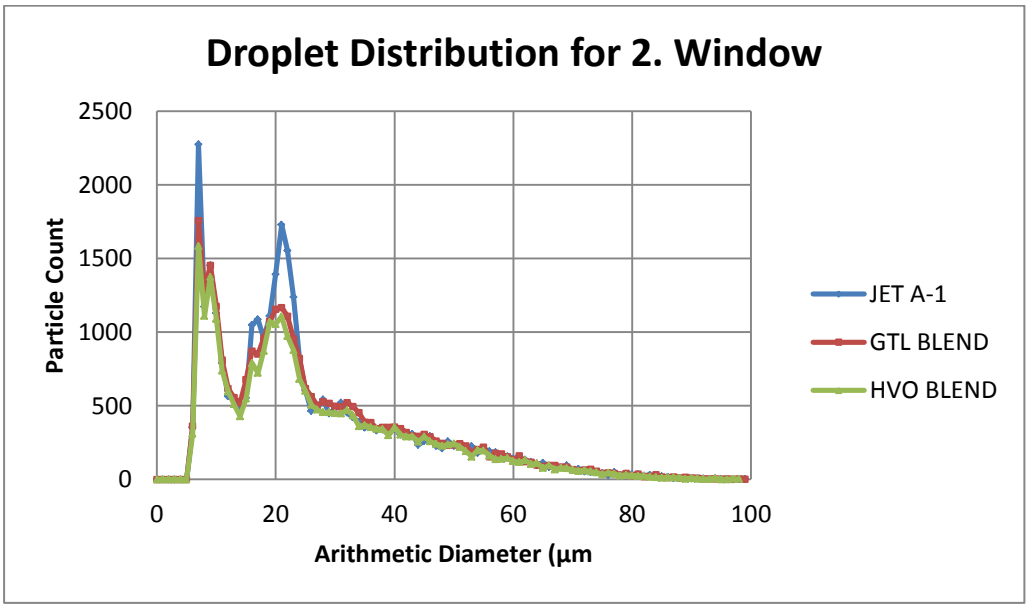

Figure 3-10 Arithmetic Droplet Distribution at 1125 kpag for 2nd Window

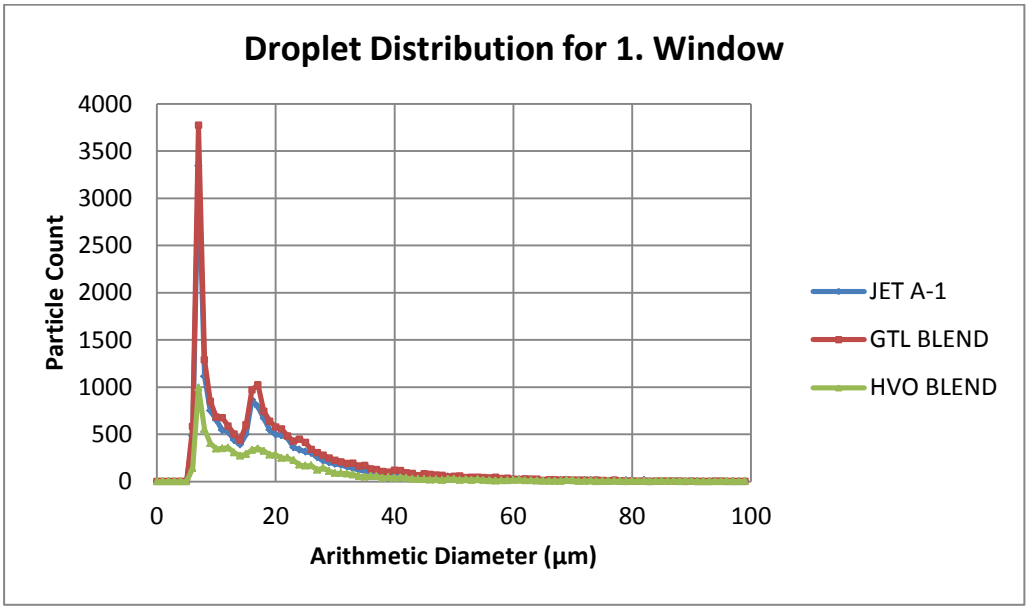

Figure 3-11 Arithmetic Droplet Distribution at 2000 kpag for 1st Window

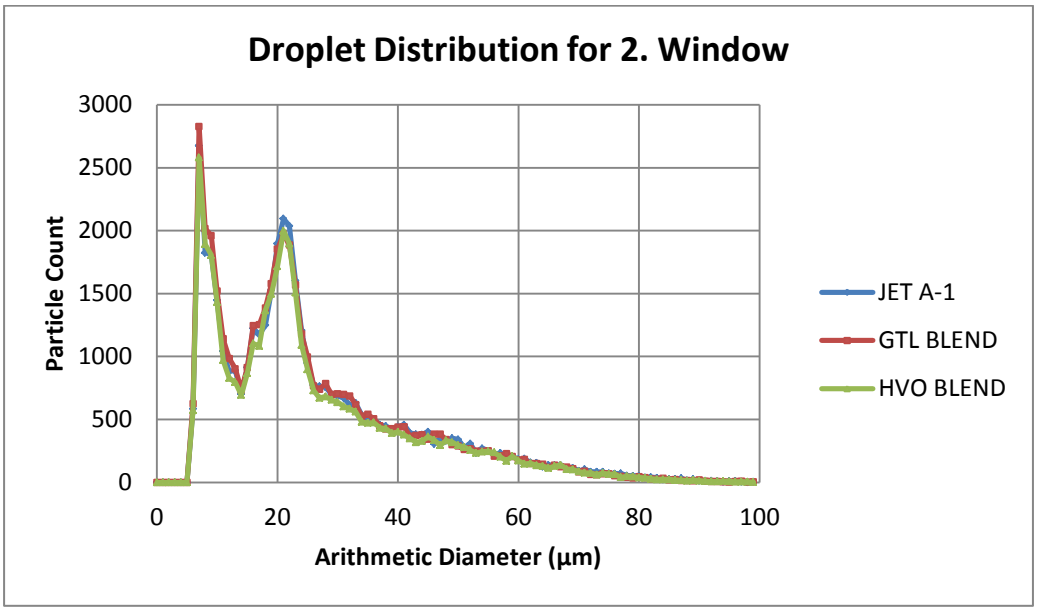

Figure 3-12 Arithmetic Droplet Distribution at 2000 kpag for 2nd Window

Spray cone angle measurements results are presented in figure 3-13. Results are non-dimensionalized according to JET A-1 cone angle at lowest fuel nozzle discharge pressure. During the pressure increment, fuel mass rate discharged from the fuel nozzle increases as well. This results in higher cone angle. GTL Blend and JET A-1 have very close cone angles during the pressure variations, whereas HVO Blend differs 1° to 4° from other fuels. Precision error in angle measurement is ± 0.5° for all fuels. However, it should be noted that errors are precision errors and the total uncertainty should be higher.

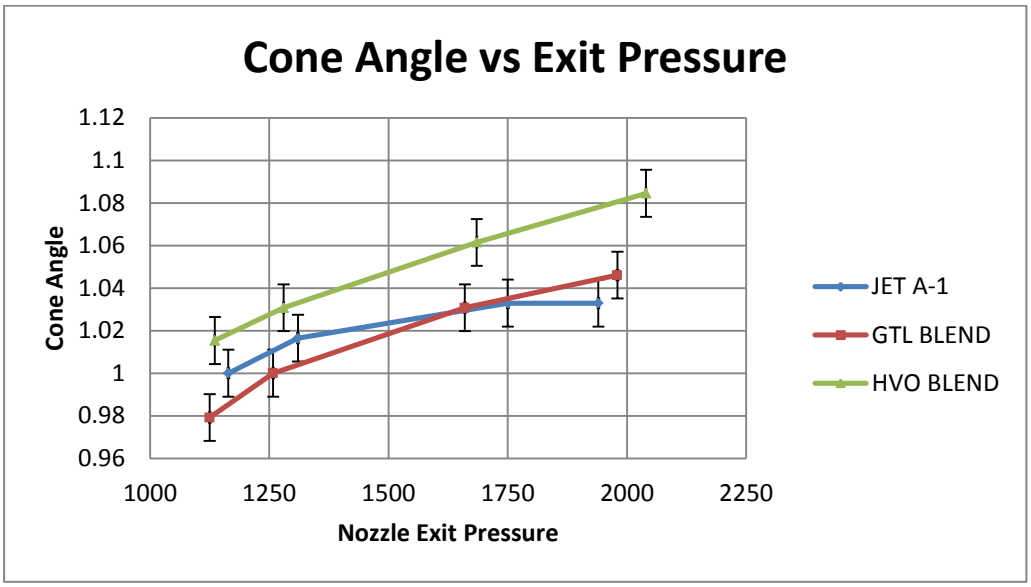

Figure 3-13 Spray Cone Angle Measurements

2-D Velocity distribution is performed by PIV method and results are displayed for 1st windows at 1150 kpag from figure 3-14 to figure 3-19. U velocity represents the velocity in x direction and V velocity represents the y direction velocity. The measurement at pressure 1750 and 2000 kpag are affected by condensed fuel spray and results do not seem reasonable.

All three fuels have almost same velocity profile. Alternative fuels have slightly lower velocities than conventional fuel. These small differences may have also been caused from slightly different fuel nozzle exit pressures.

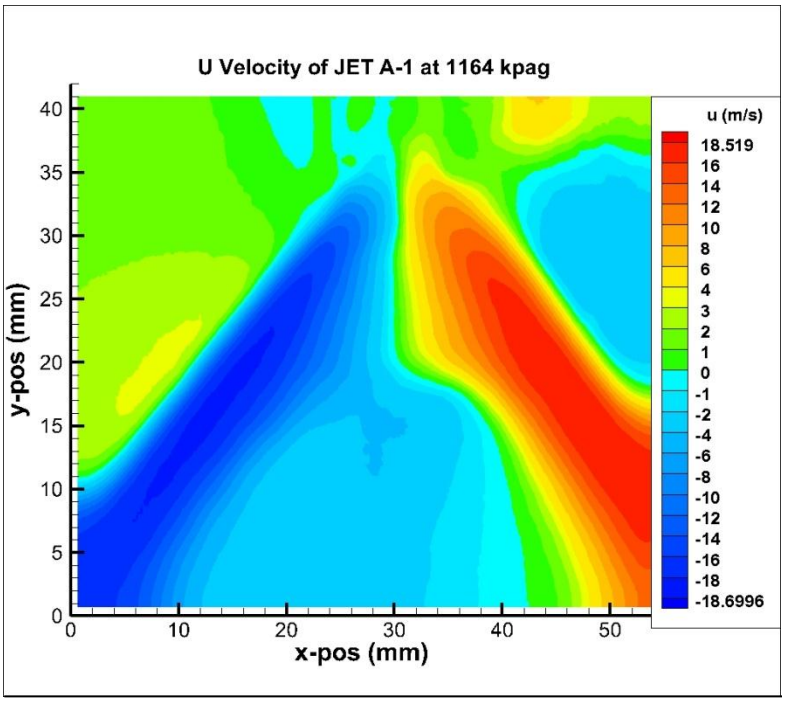

Figure 3-14 U Velocity of JET A-1 at 1164 kpag 1st Window

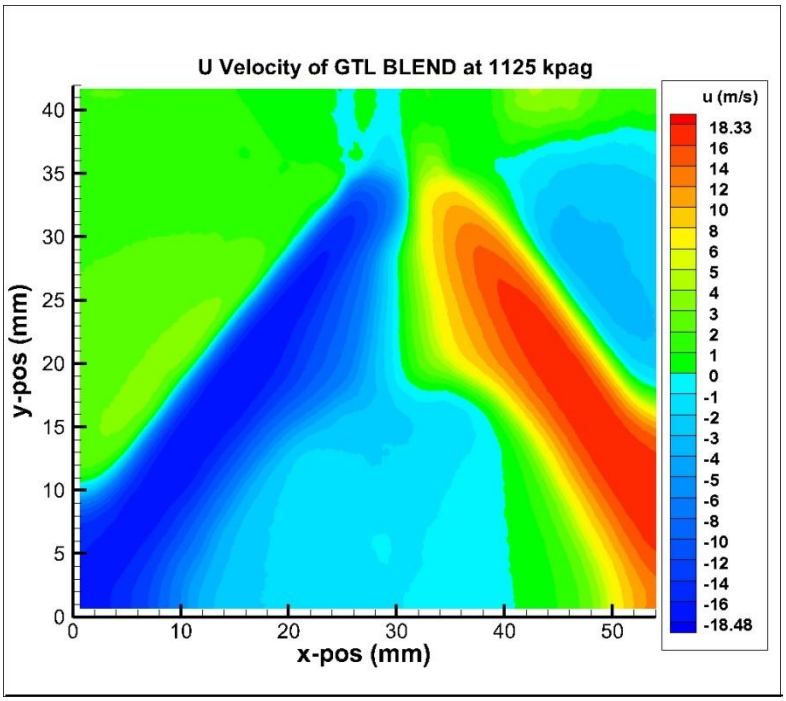

Figure 3-15 U Velocity of GTL Blend at 1125 kpag 1st Window

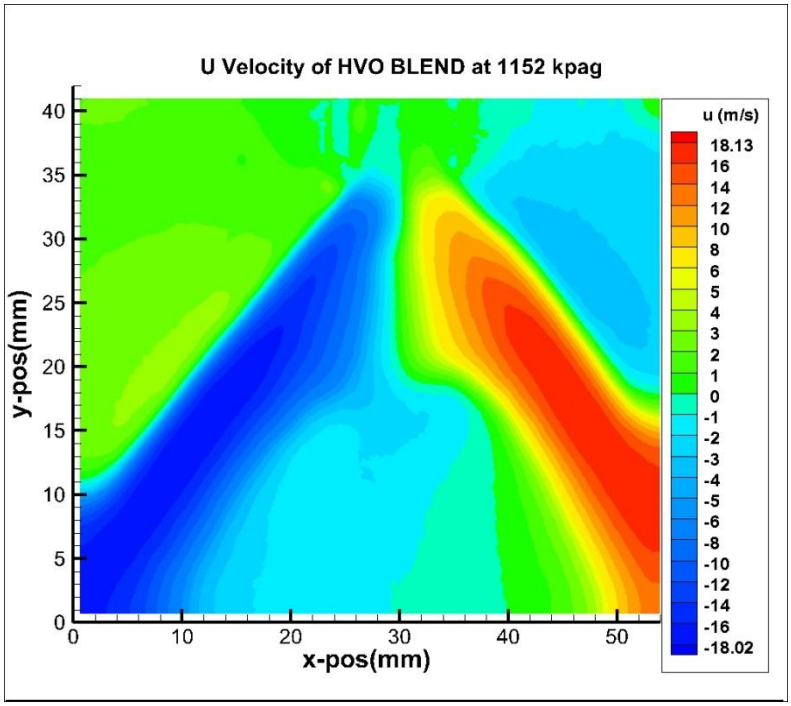

Figure 3-16 U Velocity of HVO Blend at 1152 kpag 1st Window

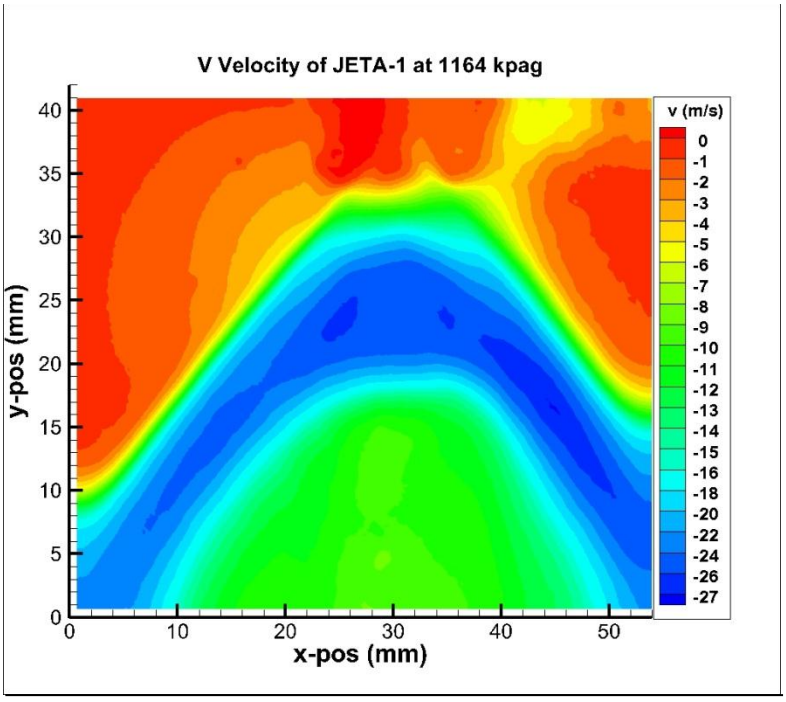

Figure 3-17 V Velocity of JET A-1 at 1164 kpag 1st Window

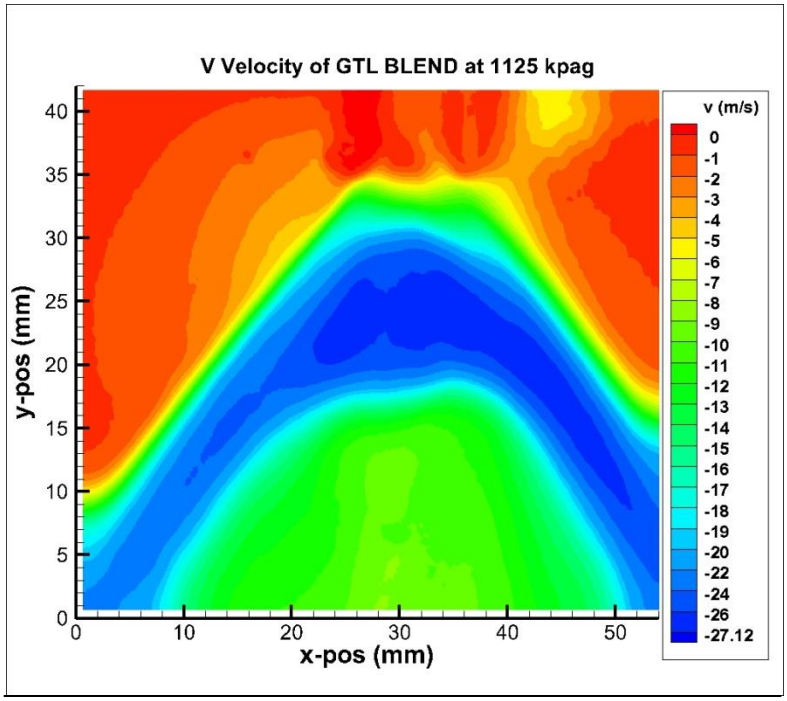

Figure 3-18 V Velocity of GTL Blend at 1125 kpag 1st Window

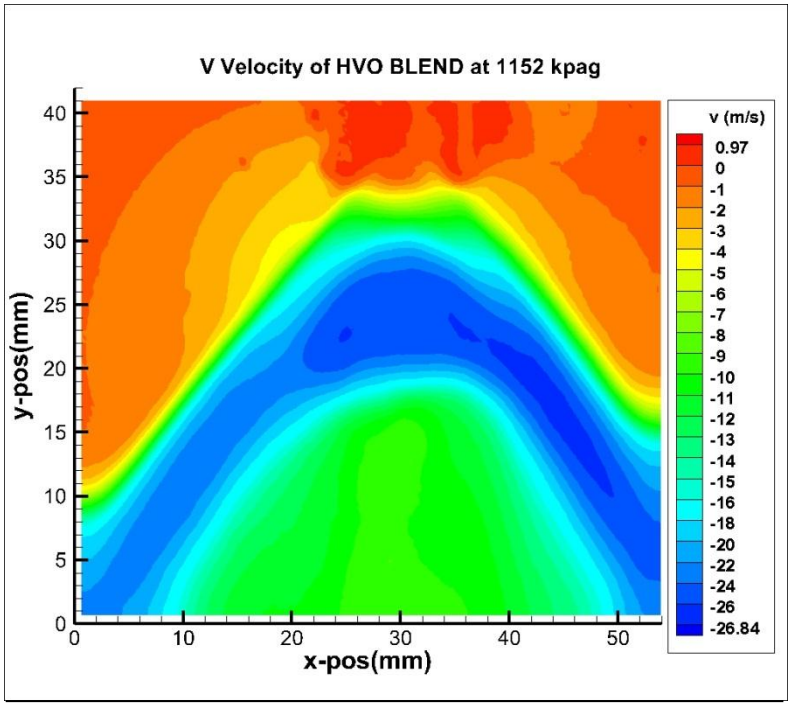

Figure 3-19 V Velocity of HVO Blend at 1152 kpag 1st Window

In conclusion, all fuel types have no major differences in terms of spray characteristics. It should be noted that spray spectrum is not only function of fuel properties but also depend on the injector geometry, exit pressure and flow rates.

The same results are measured for 1st window of 1250 kpag and 2nd window of both 1150 and 1250 kpag fuel nozzle discharge pressure. The results are displayed in Appendix B.

3.3 Results of Atmospheric Combustion Test

Exhaust gas temperature and emissions of fuels were measured at atmospheric combustion tests conditions. Results are non-dimensionalized with respect to JET A-1 values at lowest AFR.

Exhaust gas temperature in figure 3-20 , O_2 in Figure 3-21 and CO_2 levels emissions in figure 3-22 are found to be same for all fuels. Since air/fuel ratio is much smaller than typical gas turbine combustor applications and there is no air dilution, resulting emissions levels are relatively very high. Total uncertainty is ± 5 °C for exhaust gas temperature measurements, ± 0.2 % for CO_2 and O_2 emission measurements.

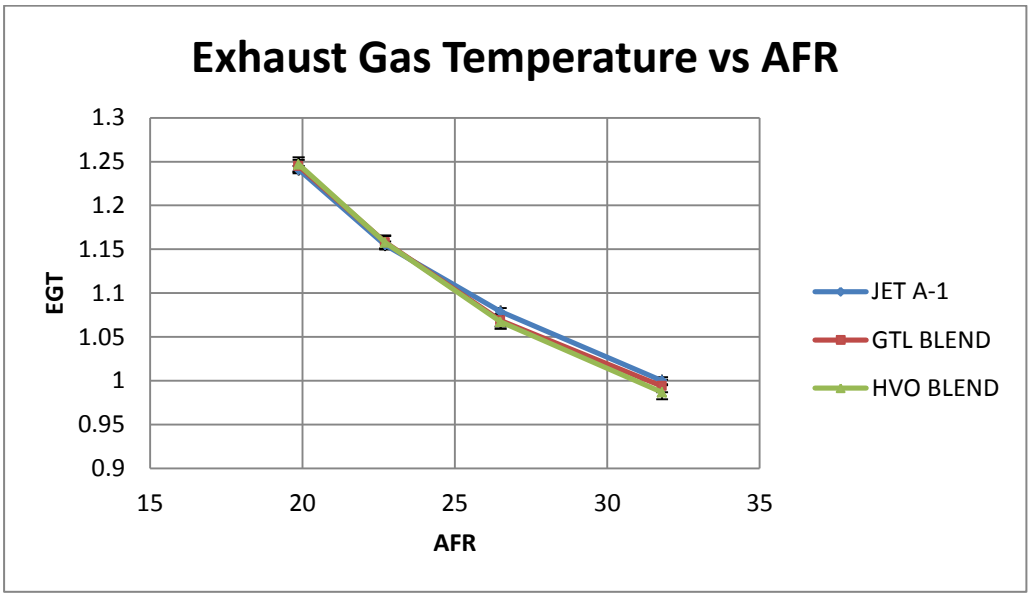

Figure 3-20 Exhaust Gas Temperature vs. AFR

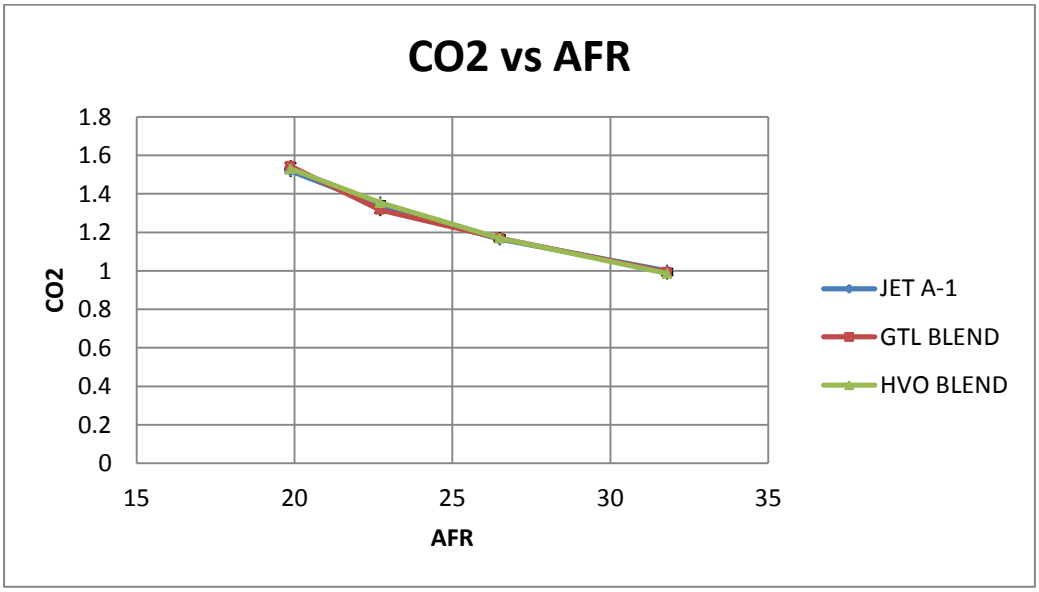

Figure 3-21 CO_2 vs. AFR

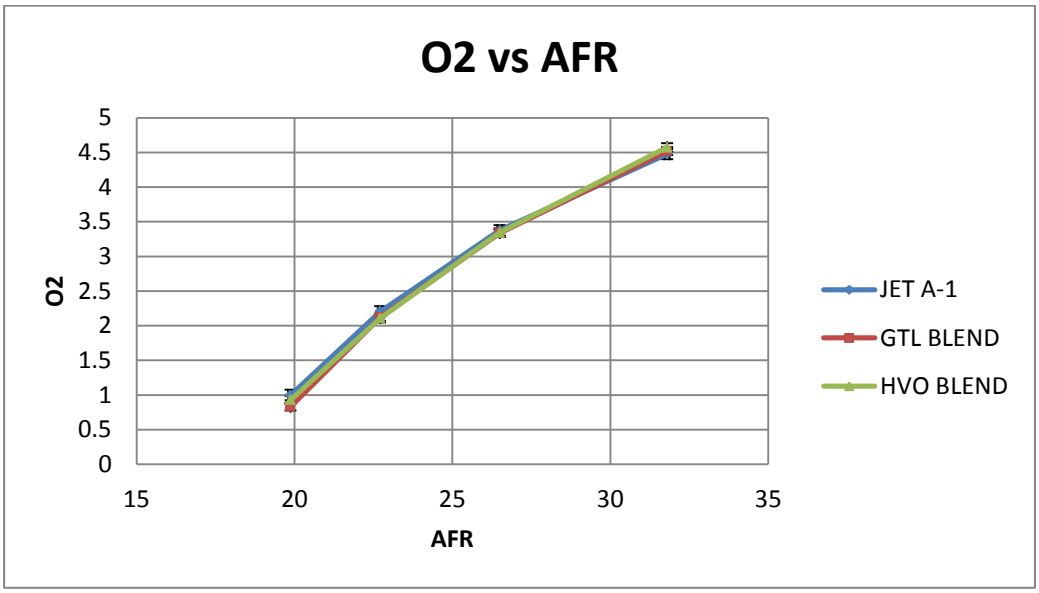

Figure 3-22 O_2 vs. AFR

CO emissions are very less for air/fuel ratio is 26.5. For air/fuel ratio 31.8, HVO blend fuel combustion has highest emissions. CO emission of JET A-1 combustion is greater than alternative fuels at lower AFRs. After exceeding air/fuel ratio 26.5, alternative fuels blend combustion have more CO emissions with respect to JET A-1 as depicted in figure 3-23. Total uncertainty in CO emission is ± 2 ppm.

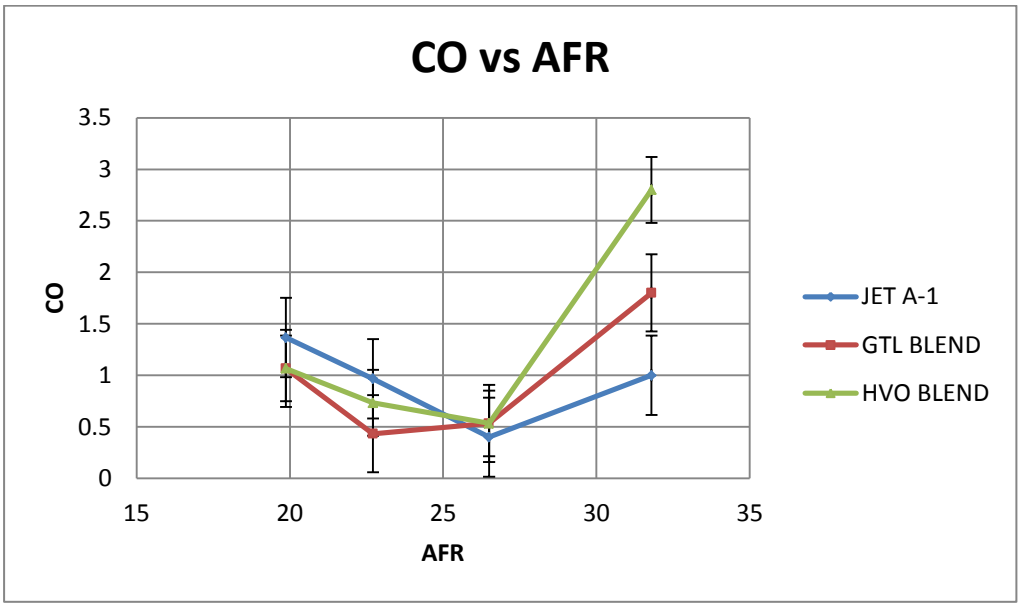

Figure 3-23 CO vs. AFR

Alternative fuels improve the total NOx emission as 2 ppm than JET A-1 during all AFR as depicted in figure 3.24. But total uncertainty is around ± 2 ppm, therefore this difference may be resulted from the measurement uncertainty.

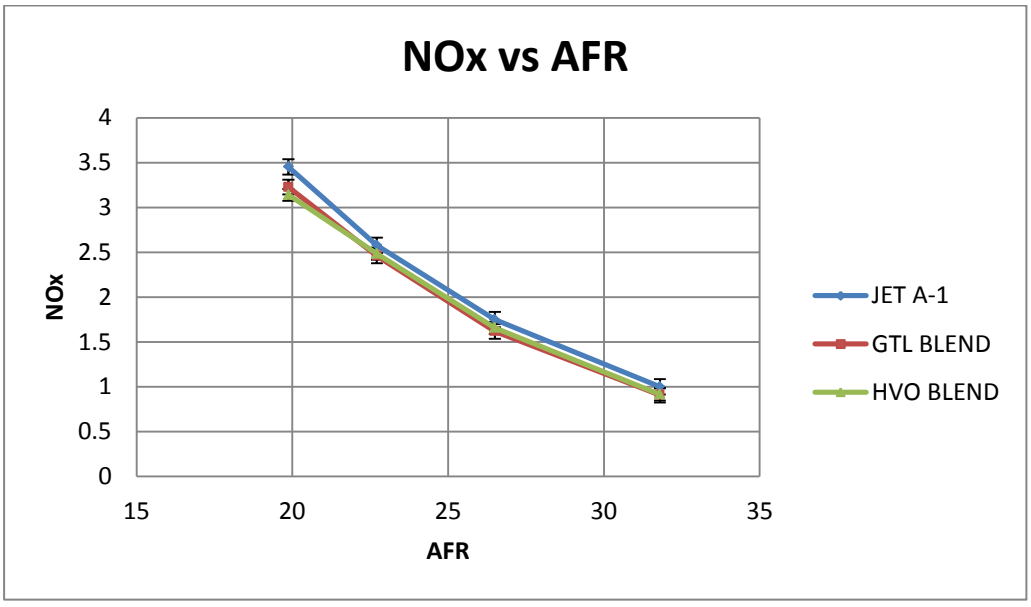

Figure 3-24 NOx vs. AFR

Figure 3.25 gives the SO_2 emission results. GTL blend has almost zero SO_2 emission. JET A-1 has correspondingly an SO_2 emission level inversely proportional to consumed fuel. HVO blend has highest SO_2 emissions proportional to consumed fuel amount. This behaviour is expected for GTL blend due to content of synthetic fuel, while these results are not expected for HVO blend.

H_2 emission is not involved due to high experimental uncertainty.

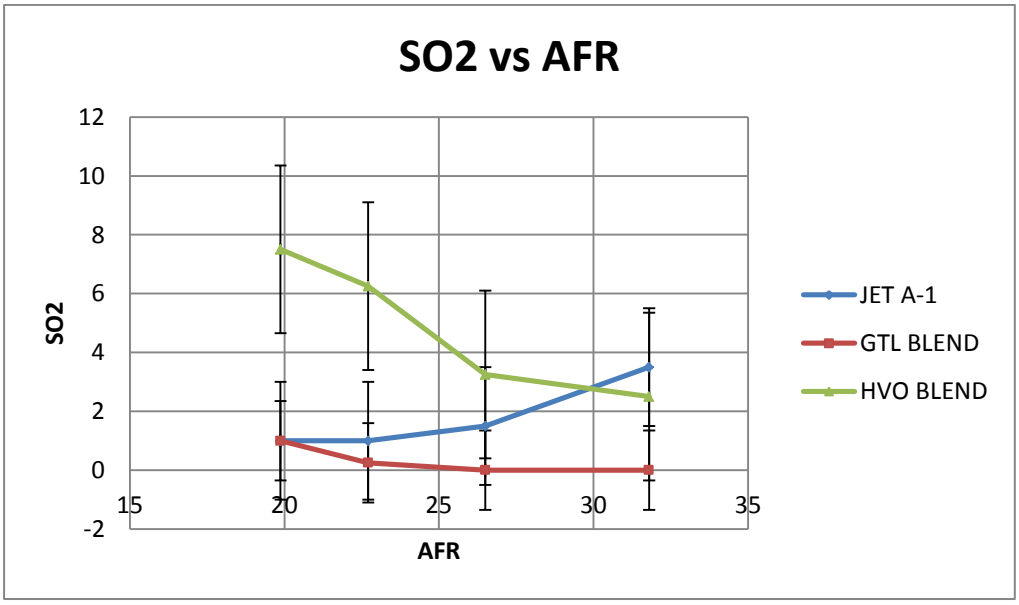

Figure 3-25 SO_2 vs. AFR

3.4 Results of Experimental Turbojet Test

Fuel/Air ratio, burner efficiency, specific thrust and specific fuel consumption are measured. The results are normalized with respect to JET A-1 result at 35000 rpm.

According to figure 3-26, JET A-1 fuel-to-air ratio is slightly greater than alternative fuels. Burner efficiency of GTL blend fuel combustion is clearly higher than the two other fuels combustions as depicted in figure 3-27. JET A-1 and HVO blend has almost same burner efficiency at low and high fuel-to-air ratios.

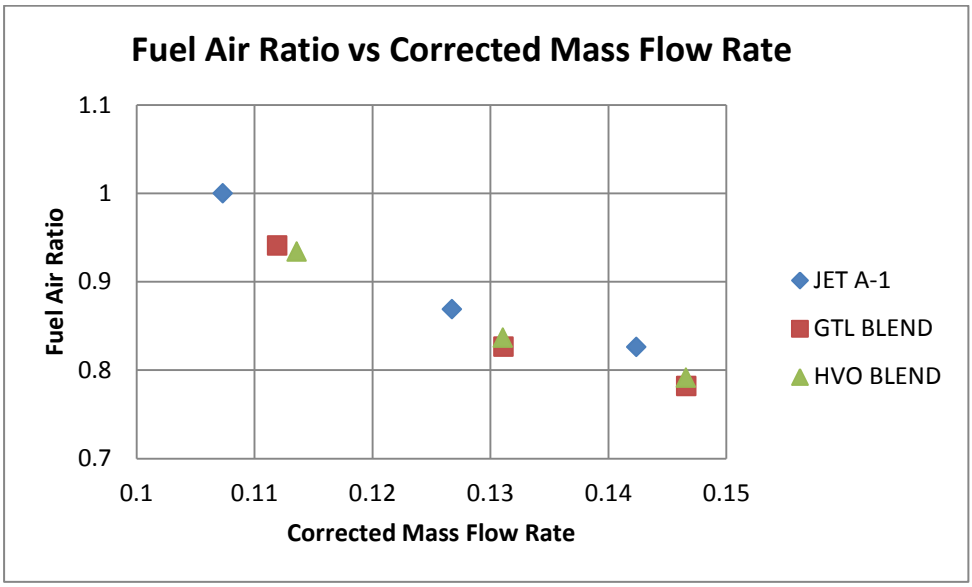

Figure 3-26 Fuel Air Ratio vs. Corrected Mass Flow Rate

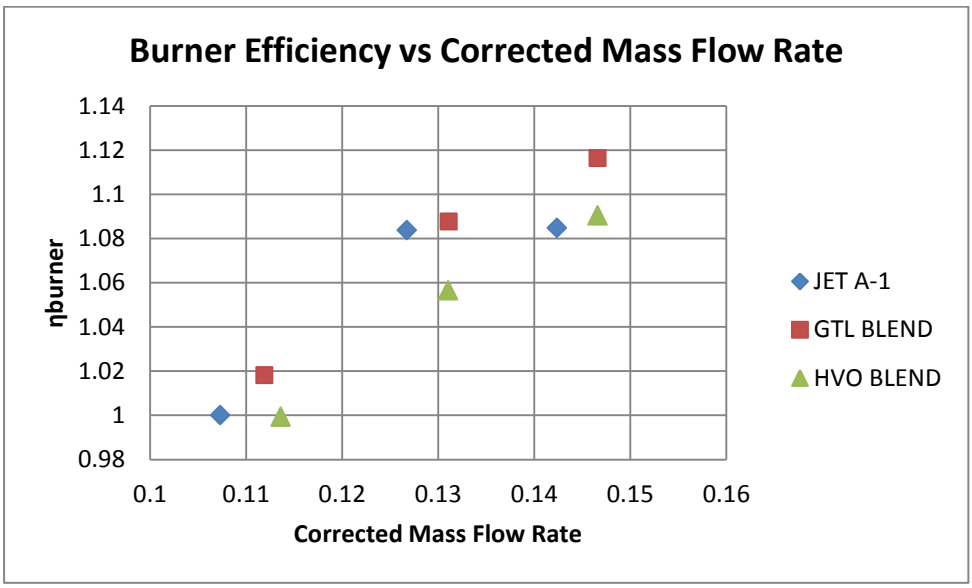

Figure 3-27 Burner Efficiency vs. Corrected Mass Flow Rate

The specific fuel consumption of both alternative fuels is slightly less than reference JET A-1 fuel combustion as seen from figure 3-28. All fuels have similar specific thrust levels as shown in figure 3-29. GTL blend shows a slight advantage in terms of burner efficiency and fuel consumption, however these differences are very small and no significance effect on overall engine performance is observed.

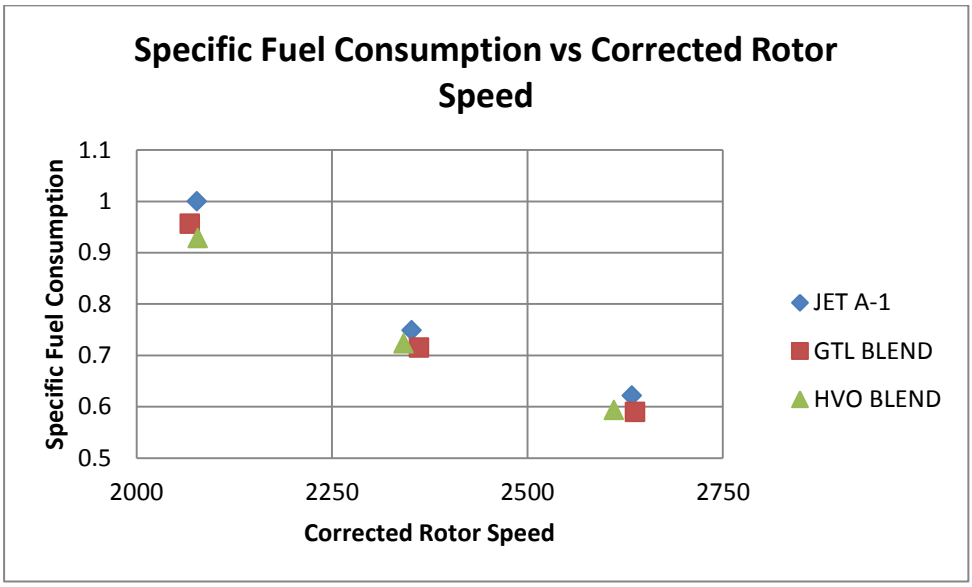

Figure 3-28 Specific Fuel Consumption vs. Corrected Rotor Speed

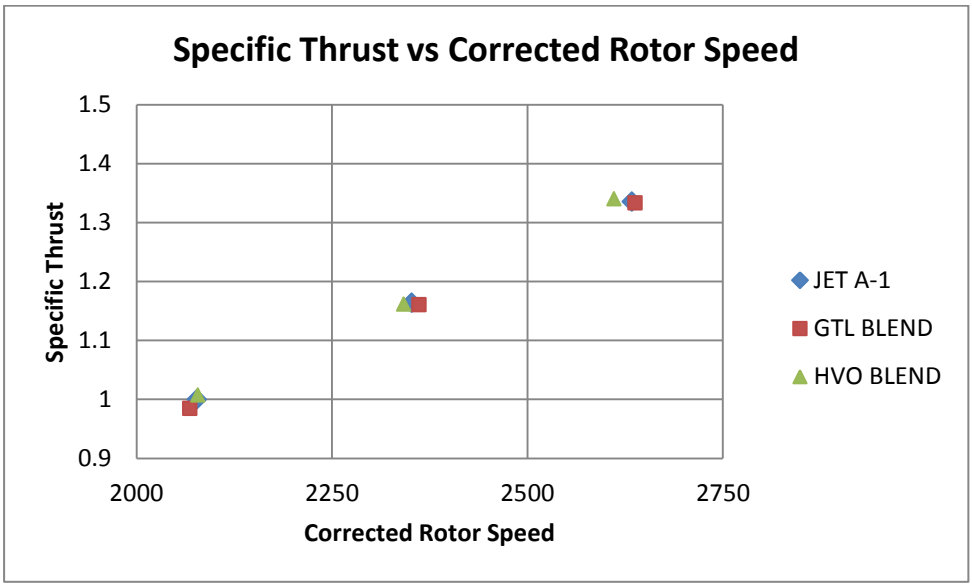

Figure 3-29 Specific Thrust vs. Corrected Rotor Speed

The specific thrust is calculated as equation 3.1.

$$Specific\ Thrust = a_0 \left\{ (1+f)\left(M_0 \frac{V_9}{V_0}\right) - M_0 + \frac{(1+f)T_9/T_0}{\gamma_c[M_0(V_9/V_0)]} \right\} \quad (3.1)$$

3.5 Results of RR 250 C-18 Turbo-shaft Engine Test

Temperature distributions at the combustion chamber exit are displayed from Figure 3-30 to Figure 3-38 for different axis. The results are non-dimensionalized with respect to average liner temperature at ground-idle start-up of JET A-1 combustion. For axis one, alternative fuel combustion yield higher liner temperature on one side only while JET A-1 combustion have high edge temperature at axis 3. This unsymmetrical behavior is not seen at measurement axis 2. 100 % HVO and GTL fuels are also examined at ground-idle start up at axis 2 and same temperature distribution is measured. Fuels have almost same behavior and the temperature differences can be negligible.

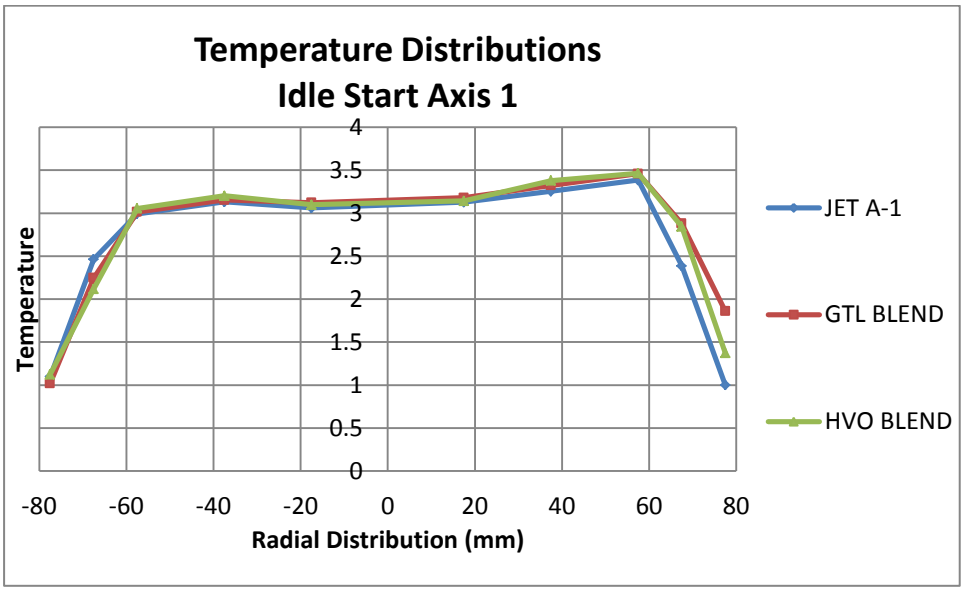

Figure 3-30 Temperature Distribution at Ground-Idle Start-up Axis 1

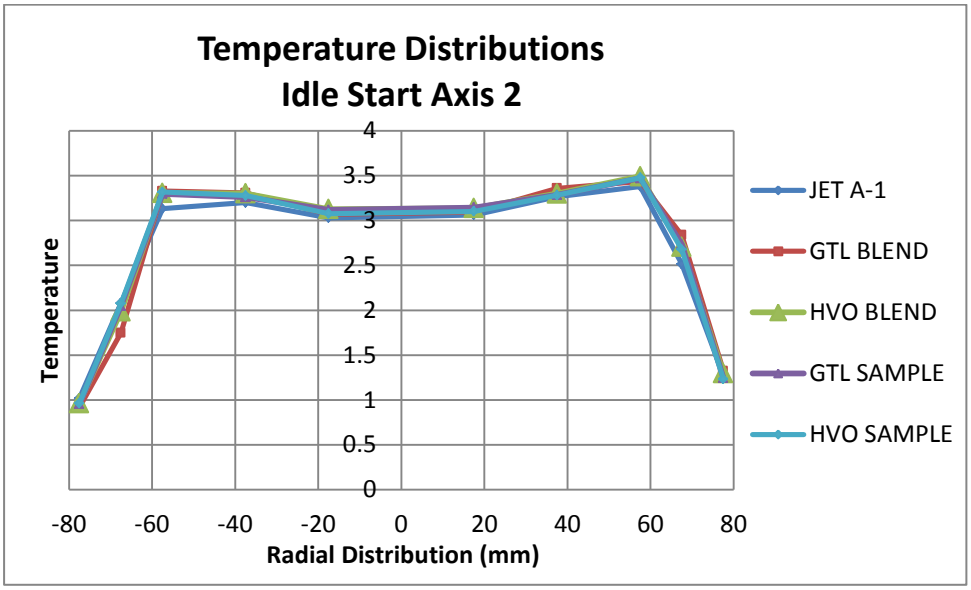

Figure 3-31 Temperature Distribution at Ground-Idle Start-up Axis 2

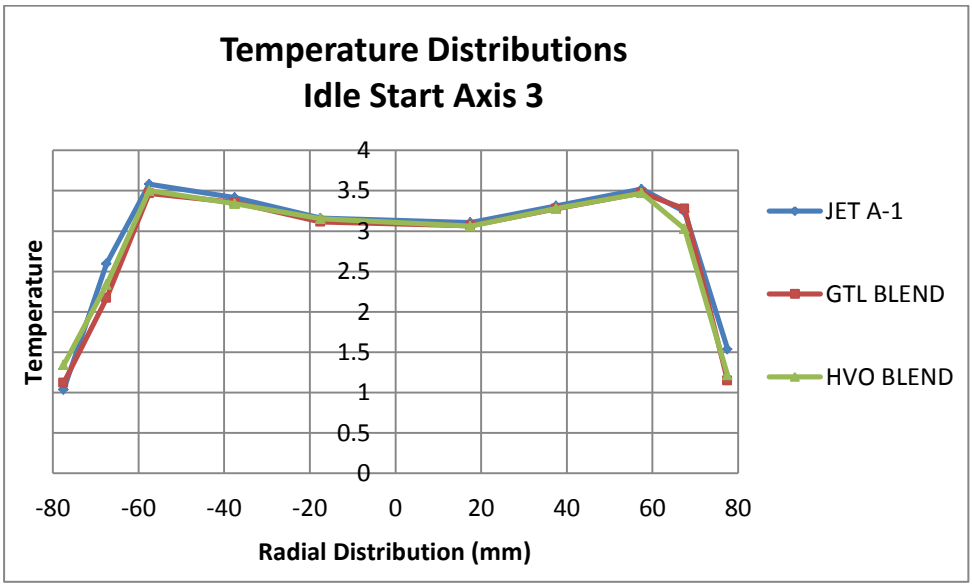

Figure 3-32 Temperature Distribution at Ground-Idle Start-up Axis 3

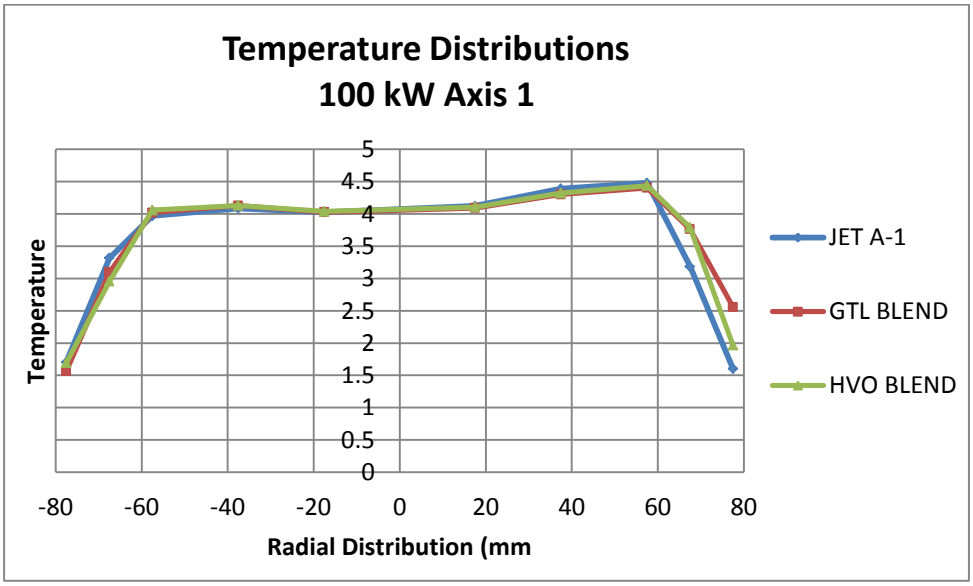

Figure 3-33 Temperature Distribution at 100 kW Axis 1

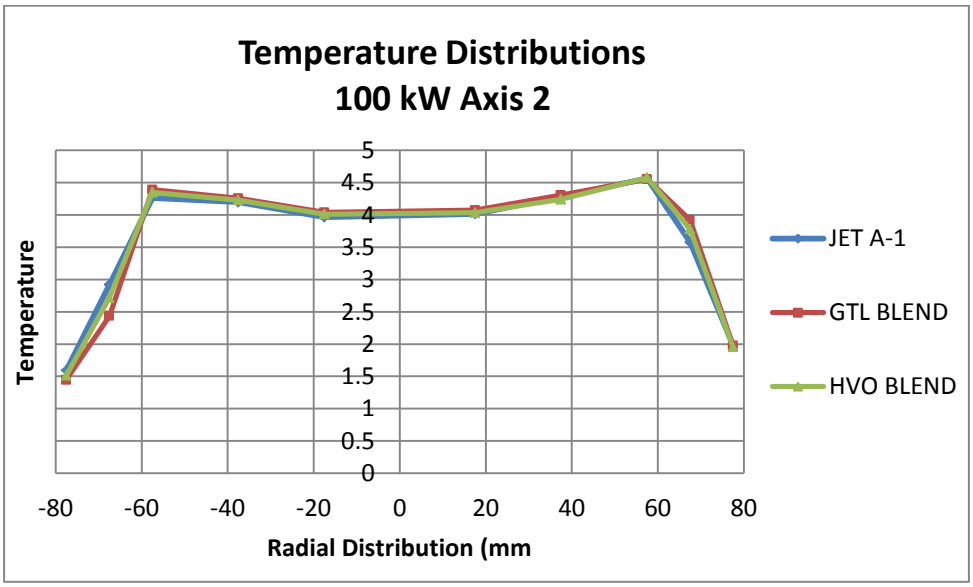

Figure 3-34 Temperature Distribution at 100 kW Axis 2

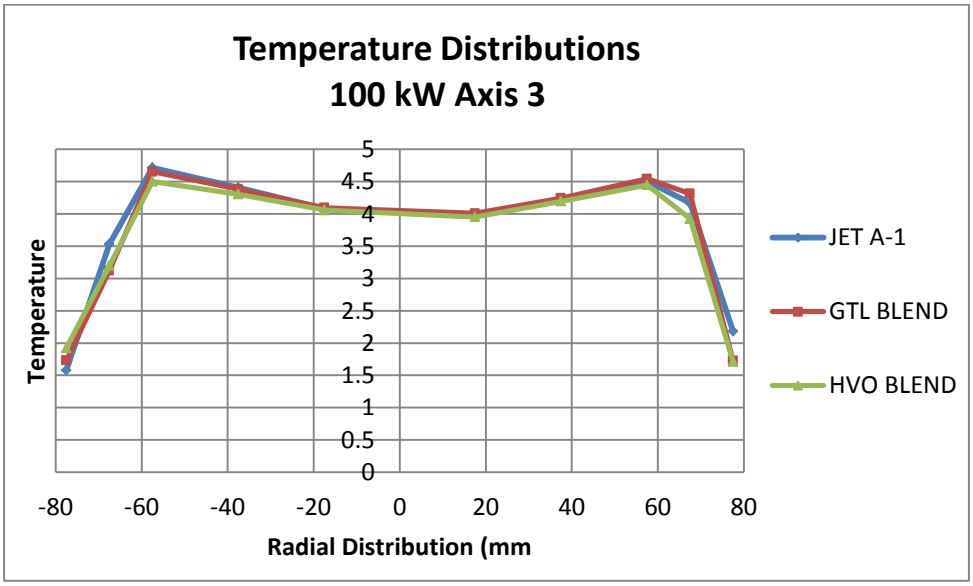

Figure 3-35 Temperature Distribution at 100 kW Axis 3

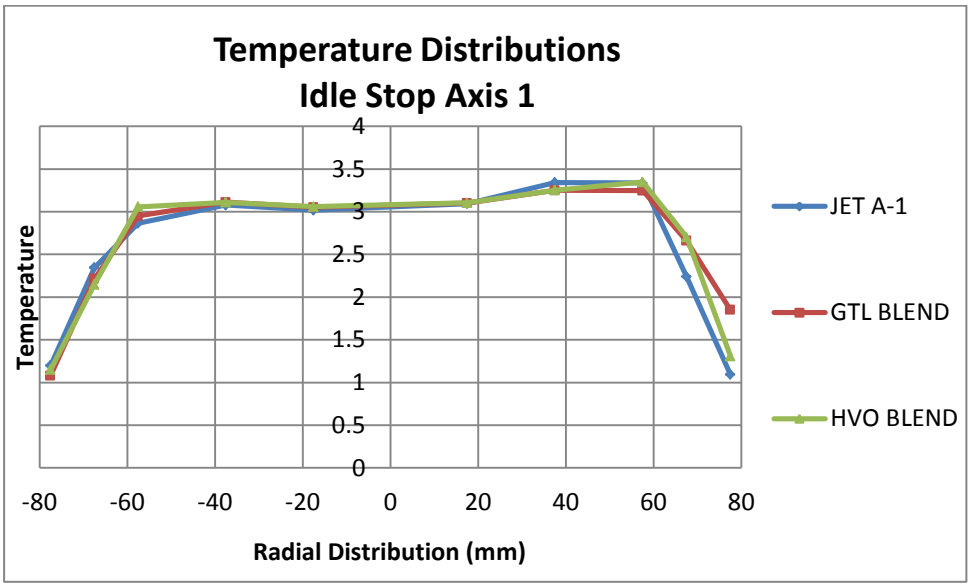

Figure 3-36 Temperature Distribution at Ground-Idle Stop Axis 1

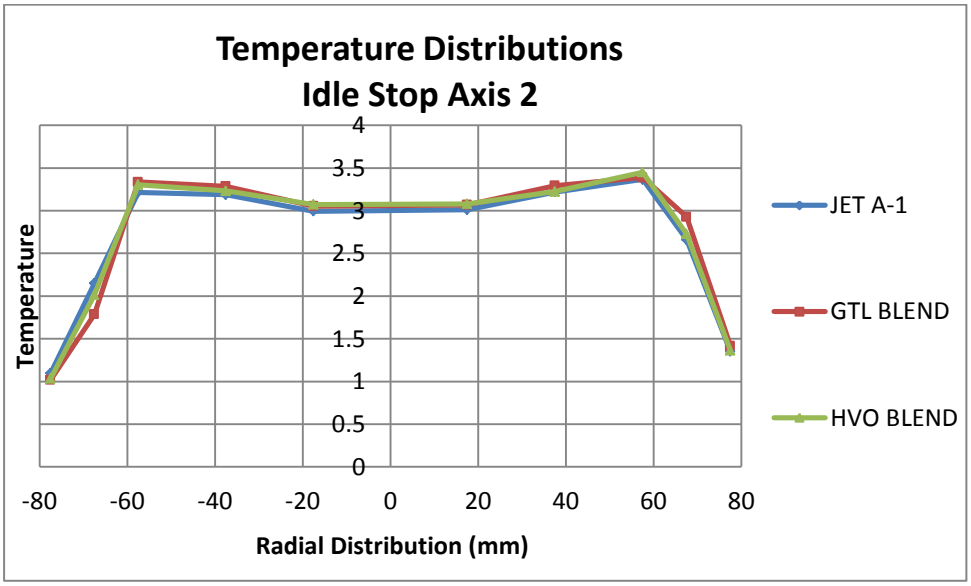

Figure 3-37 Temperature Distribution at Ground-Idle Stop Axis 2

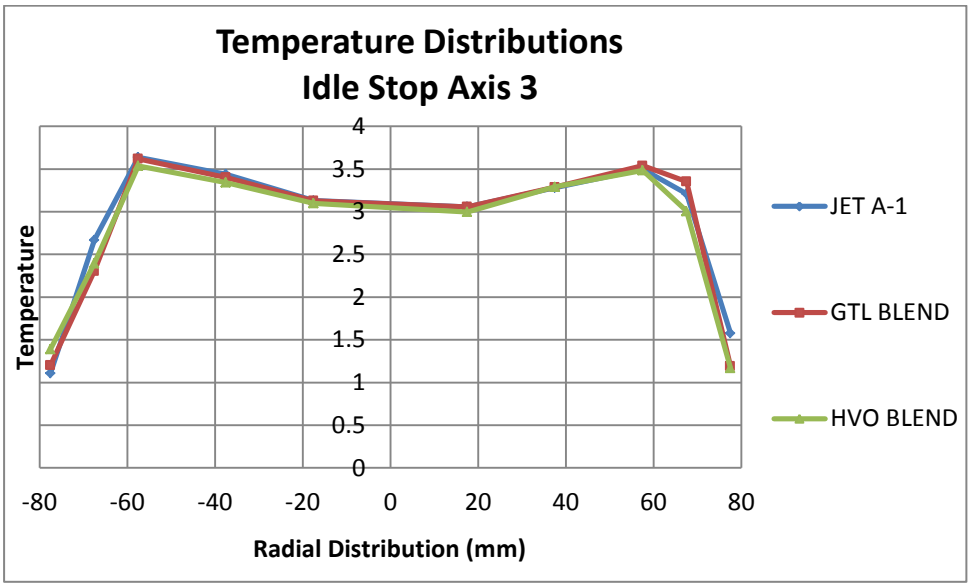

Figure 3-38 Temperature Distribution at Ground-Idle Stop Axis 3

Power turbine inlet temperature is given in Figure 3-39. This temperature is important for shaft power calculation. Except ground-idle start up, average power turbine inlet temperatures are almost same for all fuel types.

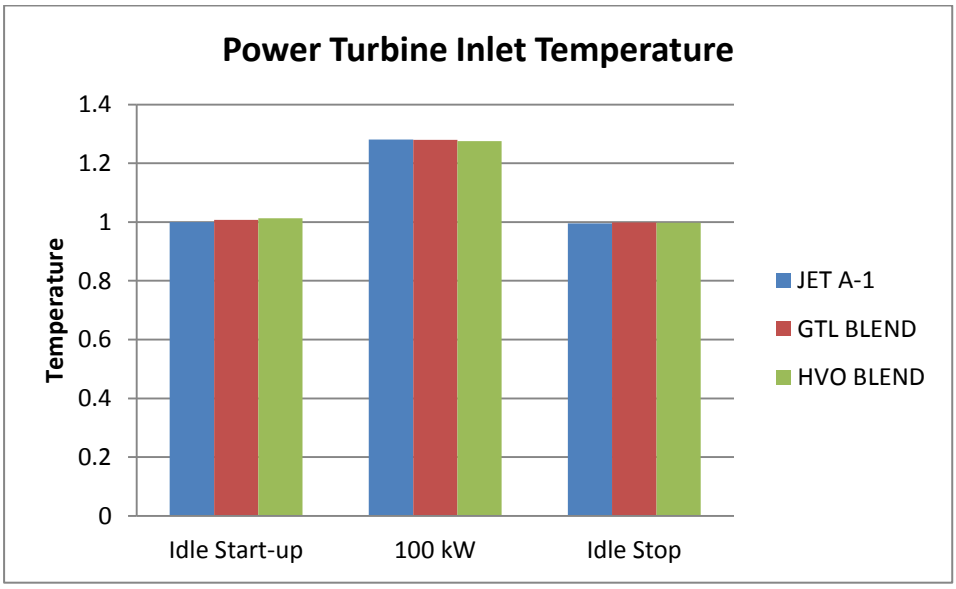

Figure 3-39 Power Turbine Inlet Temperature

JET A-1 has lowest exhaust gas temperature as depicted in Figure 3-40 . With power turbine inlet temperature, the expansion with JET A-1 combustion is greater than the alternative fuels. This implies that the shaft power with JET A-1 is greater than alternative fuels. Table 3.1 gives the shaft power results. This results are tried to be get by holding the fuel consumption as same. Fuel flow random error is order of $\pm 10^{-2}$ (g/s) and instrument error is 0.5 % of full scale and it corresponds to approximately ±0.1 g/s. Therefore, total uncertainty is ±0.1 g/s. For power uncertainty, torque total uncertainty is ±5 Nm and shaft speed is ±60 rpm. Total power uncertainty is very small such as 0.03 kW and can be negligible. Using alternative fuels has an disadvantage of 1-1.5 % shaft power loss according to results.

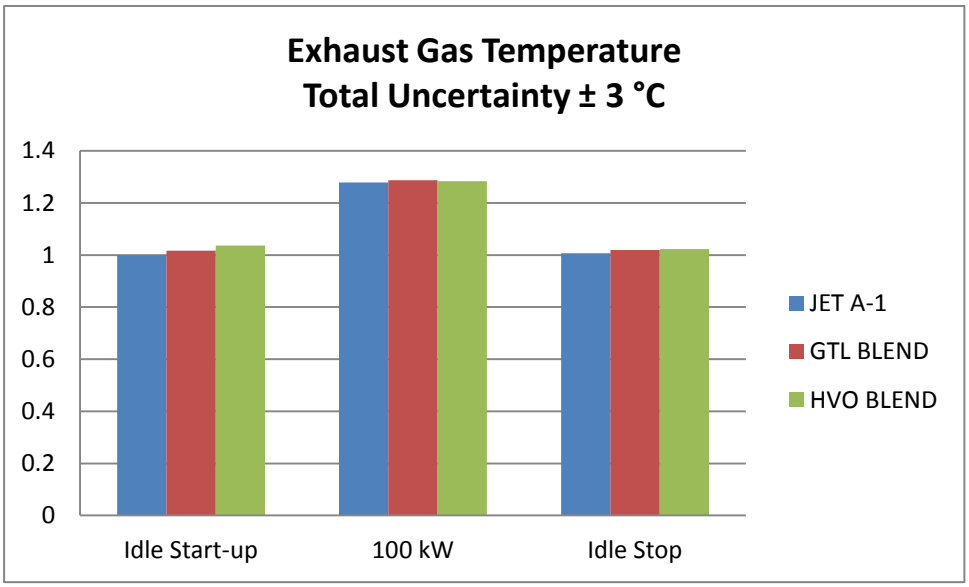

Figure 3-40 Exhaust Gas Temperature

Table 3-1 Shaft Power Measurement Results

FUEL TYPE	POWER (normalized by JET A-1)	FUEL CONSUMPTION (normalized by JET A-1)
JET A-1	1	1
GTL BLEND	0.983	1.005
HVO BLEND	0.987	1.01

Figure 3.41 shows that O_2 emission of JET A-1 is higher than alternative fuels as 0.2% than GTL Blend and 0.3 % than HVO Blend. This means CO_2 emissions of JET A-1 is the lowest fuel as depicted in Figure 3-42. CO_2 emission is less than GTL Blend as 0.3% and HVO Blend as 0.4% for JET A-1 for all power settings. For 100 kW power settings, CO emission of JET A-1 slightly greater . But for ground idle settings CO emission of JET A-1 is greater than GTL Blend as 62-49 ppm and HVO Blend as 86-57 ppm as depicted in Figure 3.43. If both CO_2 and CO results are interpreted together, it can be concluded that GTL and HVO Blend has better combustion efficiencies than JET A-1, because they have greater CO_2 and less CO emission, but this implies that heat content of alternative fuels are less than JET A-1. Total uncertainties are ± 0.05 % for O_2, ± 0.03 % for CO_2 and ± 10 ppm for CO as depicted from Figure 3-41 to Figure 3-43.

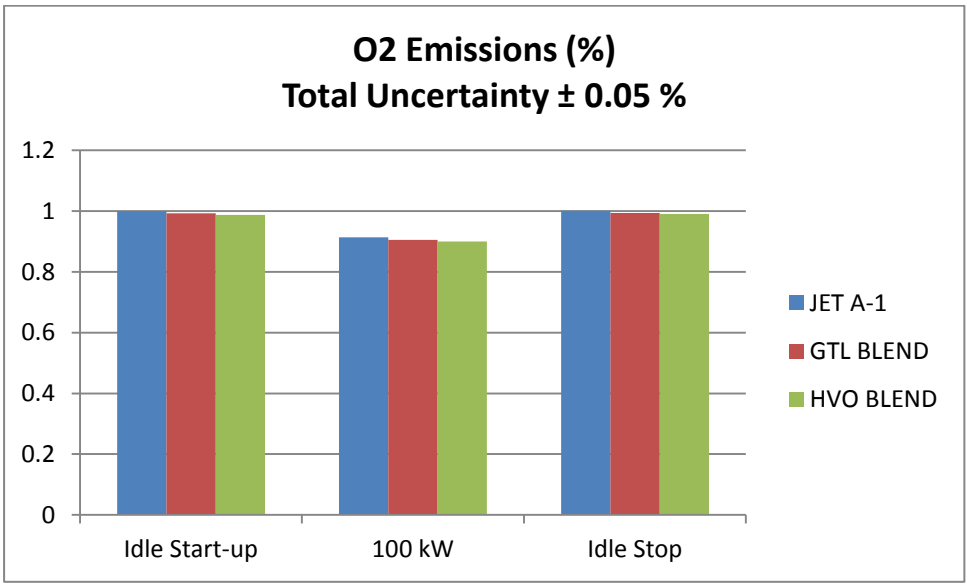

Figure 3-41 O_2 Emissions

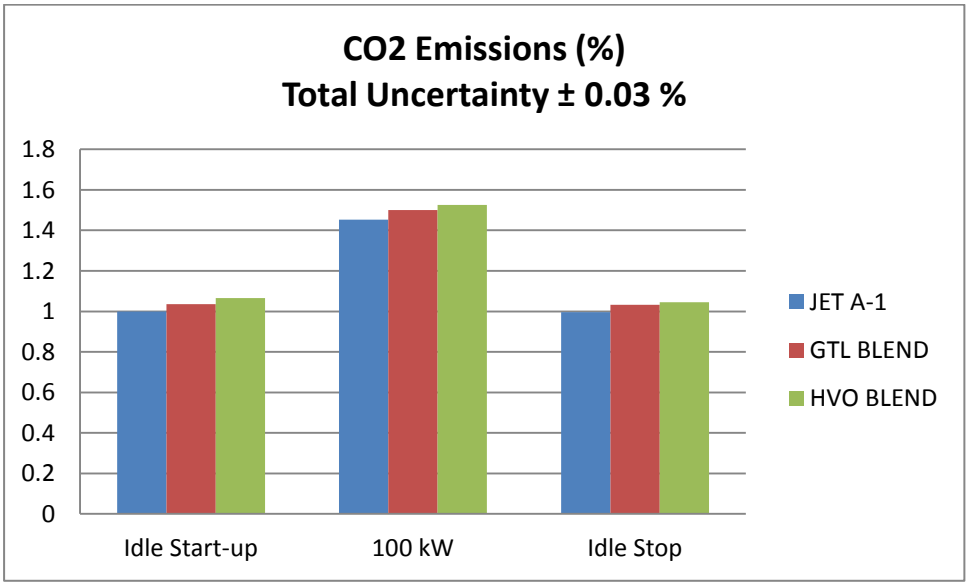

Figure 3-42 CO_2 Emissions

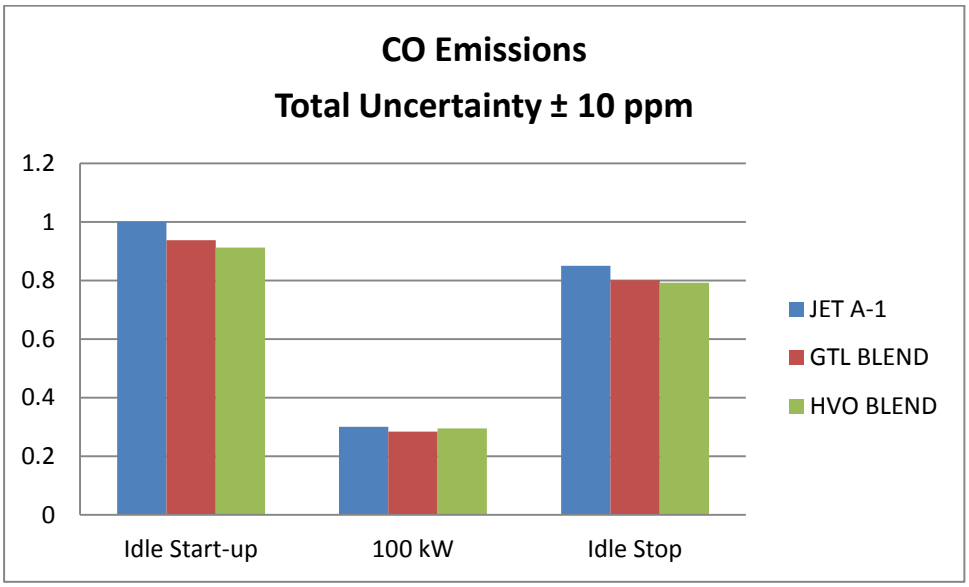

Figure 3-43 CO Emissions

There is a different situation on total NO_x emissions. Starting with NO as depicted in Figure 3-44, HVO Blend has least NO emission and difference from GTL Blend as 1-2 ppm and JET A-1 as 2-3 ppm for all power settings. In contrary to NO emission, HVO has disadvantage in NO_2 emission greater than GTL Blend as 1.5-2 ppm and JET A-1 as 2-3 ppm as depicted in Figure 3.45. Hence, total NO_x emissions of JET A-1 is less than alternative fuels as 1 ppm for ground-idle, but for 100 kW settings greater as 1 ppm alternative fuels as depicted in Figure 3-46. Because NO_x is temperature-driven and exhaust gas temperature of JET A-1 is less than alternative fuels at ground idle, NO_x emission is less, but this temperature is very close to each other for all fuels at 100 kW settings, similar behavior were measured on NO_x emission. But this differences is within the limit of total uncertainty, in other words all fuels shows almost same behavior for total NO_x emission. Total uncertainties are ±1 ppm for NO, ±0.5 ppm NO_2, ±1.5 ppm for NO_x.

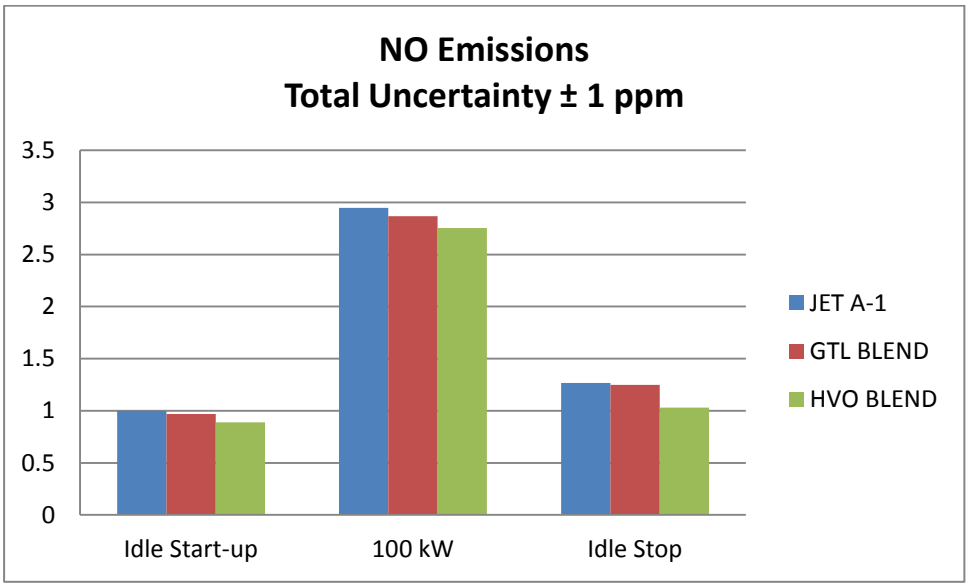

Figure 3-44 NO Emissions

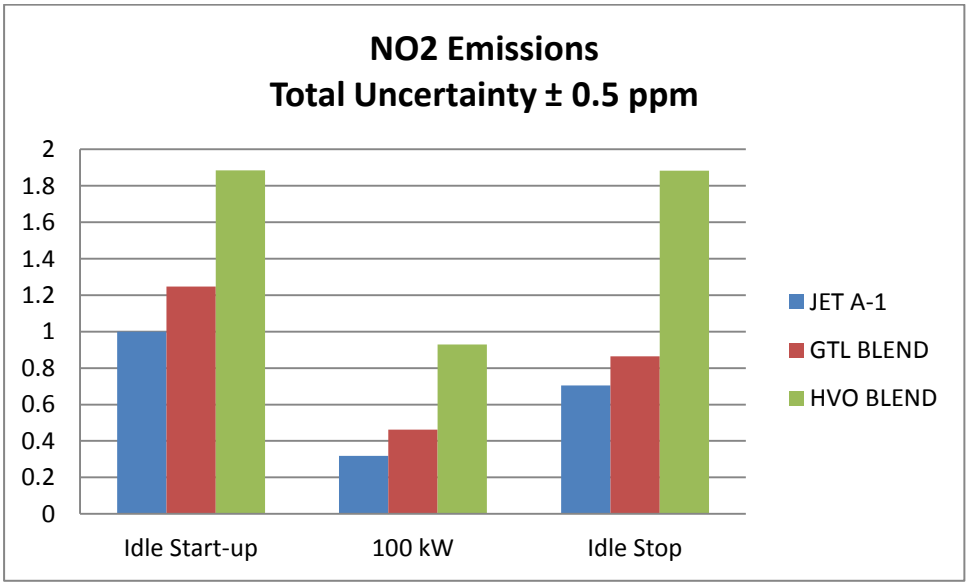

Figure 3-45 NO_2 Emissions

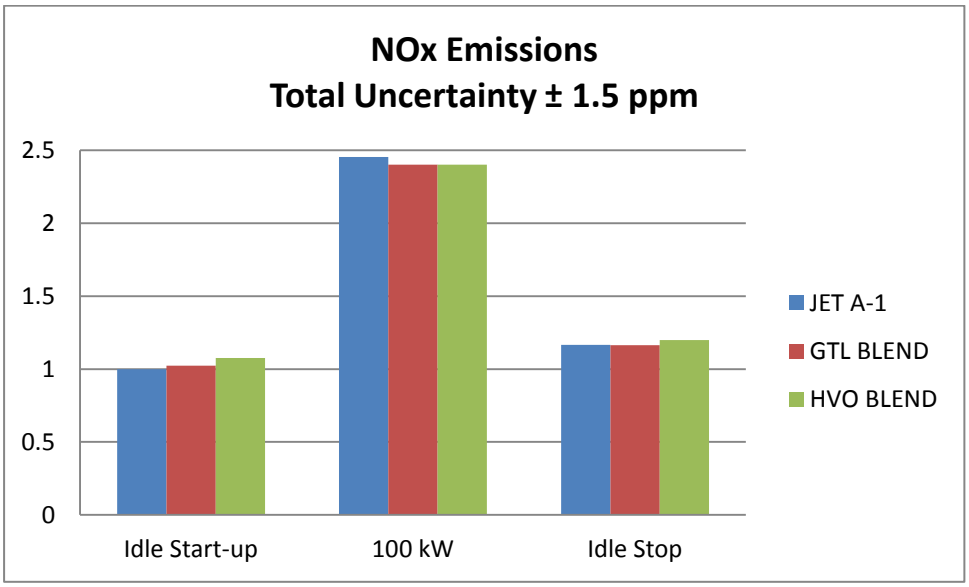

Figure 3-46 NO_x Emissions

Alternative fuels have advantage over JET A-1 for SO_2 emission. GTL Blend and JET A-1 has no SO_2 emission for 100 kW setting and HVO has very small SO_2 emission and it can be ignored. For ground-idle setting JET A-1 has greater emission. SO_2 emission of GTL and HVO Blend is caused from their blend contents with JET A-1. For H_2 emissions, the differences between fuels is 3-4 ppm and and negligible as well. Total uncertainties are ± 1 ppm for SO_2 emission and ± 5 ppm H_2 emission as depicted in Figure 3-47 and 3-48 respectively.

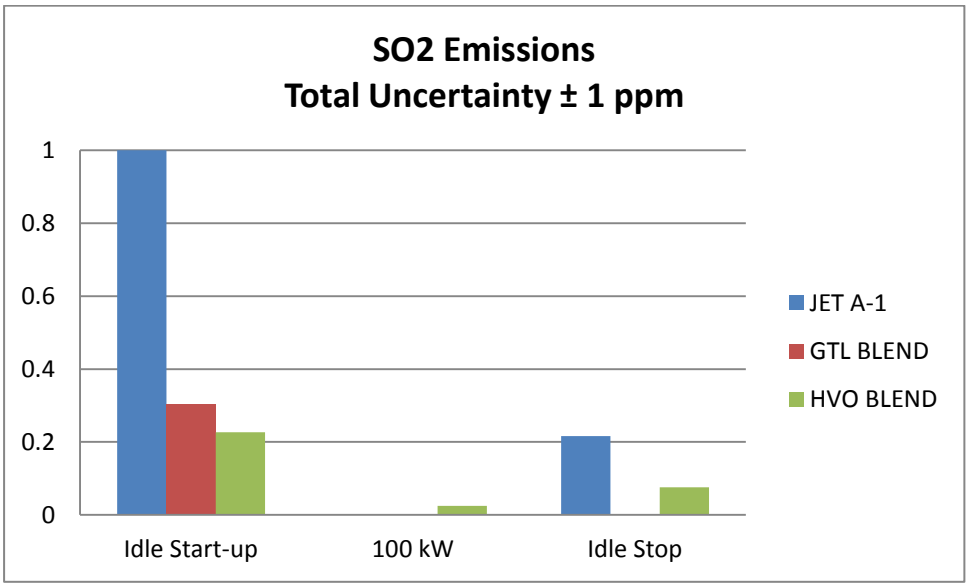

Figure 3-47 SO_2 Emissions

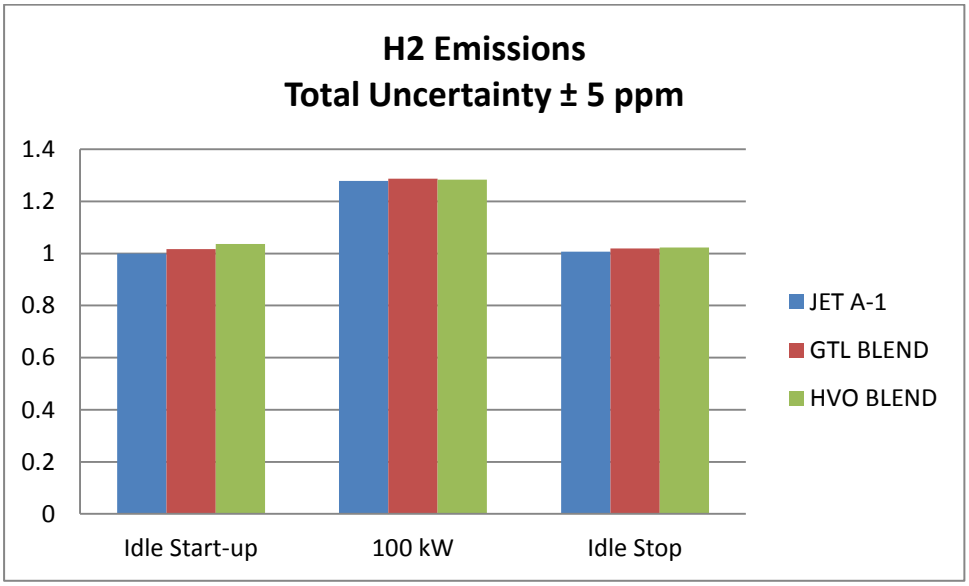

Figure 3-48 H_2 Emissions

CHAPTER 4

CONCLUSION

In this thesis, a comparative experimental study of conventional and alternative jet fuel which are GTL and HVO blended with JET A-1 as 50 %. Tests were divided into two groups cold and reacting flow tests. Cold flow tests pump and combustor injector tests were carried out at original parts of RR Allison Engine. Reacting flow tests were conducted at atmospheric combustion, experimental turbojet and RR Allison turbo-shaft tests. The tests except Allison tests were not only for monitoring the other parameters but also the preliminary tests to estimate the behavior of fuels on turbo-shaft engine and necessary modification.

Alternative fuel had similar fuel flow rate, discharge pressure with JET A-1 according to pump tests. GTL Blend had almost same property with JET A-1in terms of mean diameters and droplet distribution, while HVO blend differed from these fuel, but this differences were insignificant and it may be caused from small different fuel nozzle exit pressure. According to atmospheric combustion test, fuel showed almost same behavior in terms of exhaust gas temperature, O_2 and CO_2 emission. Some improvement in CO and NO_x had been observed but this was not significant. Contrary to expectations, HVO blend had greatest SO_2 emission. In the experimental turbojet, GTL Blend had better burner efficiency, but again this was had no significant effect on engine performance. In turboshaft experiments, 1-1.5 % loss of engine power had been measured with alternative fuel with respect to JET A-1. Alternative fuels had more CO_2, less CO emission

They had better burner efficiency, but their heat content should be less. These studies showed again that total NO_x emission strongly depends on temperature. As expected, alternative fuels especially GTL Blend had almost non-SO_2 emission at which alternative fuels had strong argument on this property. Small SO_2 emission should be resulted from blend content.

To sum up, alternative fuels had almost similar behavior with JET A-1, although they provided some improvements on emission. They offer a good candidate today aviation fuel diversity and supply even with these performances.

It should be noted that combustion property is not depend on only fuel type but also geometry that enhances the fuel air mixture.

REFERENCES

[1] Penner, J., Lister, D., Griggs, Dokken, D., McFarland, M., " Aviation and Global Atmosphere" , Cambridge University Press, 1999.

[2] Airbus, " Global Market Forecast 2008-2028" , Airbus, 2009.

[3] Srinivasan, A., Ellis, B., Crittenden, J. F., Lear, W. E., Rotavera, B., Petersen, E. L., "Fischer-Tropsch Fuel Characterization via Microturbine Testing and Fundamental Combustion Measurements", *Proceedings of ASME Turbo Expo 2008:Power for Land Sea and Air,* ASME, Berlin, 2008, GT2008-51447.

[4] Hileman, J. I., Stratton, R. W., Donohoo, P. E., "Energy Content and Alternative Jet Fuel Viability", *Journal of Propulsion and Power,* AIAA, Vol.26, No.6, 2010, pp.1184-1195.

[5] Islin, J. A., Cerza, M., Jenkins, P. E., "An Experimental Study on the Effects of Fisher-Tropsch(FT) Blends with Diesel # 2 and JP5 on the Performance of a Rollce-Royce Model 250- C20B Gas Turbine Engine", *Proceedings of ASME Turbo Expo 2010:Power for Land Sea and Air,* ASME, Glasgow, 2010, GT2010-22436.

[6] Corporan, E., DeWitt., M., J., ,Belovich, V., Pawlik, R., Lynch, A. C., Gord, J. R., Meyer, T. R., "Emissions Characterictics of a Turbine Engine and Research Combustor Burning a Fisher-Tropsch Jet Fuel", *Energy & Fuels*, Vol.21, 2007, pp. 2615-2626.

[7] Greg, P., Allan, W., Poitras, P., "Emissions from a Gas Turbine Sector Rig Operated with Synthetic Aviation and Biodiesel Fuel", *Proceedings of ASME Turbo Expo 2010:Power for Land Sea and Air,* ASME, Glasgow, 2010, GT2010-22494.

[8] Nguyen, D. N., Ishıda, H., Shioji, M., "Gas to Liquid Sprays at Different Injection and Ambient Conditions", *Journal of Engineering for Gas Turbines and Power*,ASME, Vol.33, No.3, 2011, pp. 032804.

[9] Speight, J. G., "The Chemistry and Technology of Petroleum", CRC Press, 2006.

[10] Bogers, P., "Industry Options & Challenges", *Aviation and Alternative Fuels,* ICAO, Montreal, Canada, 2009.

[11] PARTNER "U.S. Fuel Trend Analysis", *Fourth Meeting of the Group on International Aviation and Climate Change* , May 2009 Montreal, Canada.

[12] Jones, E. G., Balster, L. M., Balster, W. J., "Autooxidation of Neat and Blended Aviation Fuels", *Energy & Fuels,* Vol.12, 1998, pp. 990-995.

[13] Lefebvre, A. H., Ballal, D. R., "Gas Turbine Combustion Alternative Fuels and Emissions", CRC Press, 2010.

[14] Moses, C. A., "Comparative Evaluation of Semi-Synthetic Jet Fuels", Coordinating Research Council , Rept. AV-2-04a, Alpharetta, GA, Sept. 2008.

[15] Goodger, E., Vere, R., "Aromatics Fuels", *Aviation Fuel Technology,* MacMillan, 1985.

[16] Hemighaus, G., Boval, T., Bosley, C., Organ, R., Lind, J., Broutte, R., Thompson, T., Lynch, J., Jones, J., "Alternative Jet Fuels", *Aviation Fuel Technical Review,* FTR-3/A1, 2006.

[17] DeWitt, M. J., Corporan, E., Graham, J., Minus, D., "Effects of Aromatic Type and Concentration in Fischer-Tropsch Fuel on Emissions Production and Material Compatibility", *Energy & Fuels*, Vol.22, 2008, pp.2411-2418.

[18] Blakey, S., Rye, L., Wilson, C. W., "Aviation Gas Turbine Alternative Fuels: A Review", *Proceedings of Combustion Institute,* Vol.33, 2011, pp. 2863-2885.

[19] Moses, C. A., Roets, P. N. J., "Properties, Characteristics and Combustion Performance of Sasol Fully Synthetic Jet Fuel", *Journal of Engineering for Gas Turbines and Power,* ASME Vol.131, No.4, 2009, pp. 041502.

[20] Bulzan, D., Anderson, B., Wey, C., Howard, R., Winstead, E., Beyersdorf, A., Corporan, E., DeWitt, M. J., Klingshirn, C., Herndon, S., Lye, R. M., Timko, M., Wood, E., Tacina, K. M., Liscinksy, D., Hagen, D., Lobo, P.,

Whitefield, P., "Gaseous and Particulate Emissions Results of the NASA Alternative Fuel Experiment (AAFEX)", *Proceedings of ASME Turbo Expo 2010:Power for Land Sea and Air,* ASME, Glasgow, 2010, GT2010-23524.

[21] Corporan, E., DeWitt, M. J., Klingshirn, C.D., Striebich, R., Cheng, M.D.,"Emissions Characteristics of Military Helicopter Engines with JP-8 and Fischer-Tropsch Fuels", *Journal of Propulsion and Power,* AIAA, Vol.26, No.2, 2010, pp.317-324.

[22] International Coordinating Council of Aerospace Industries Association, "Impact of Alternative Fuels on Aircraft Engine Emissions", *Aviation and Alternative Fuels,* ICAO, Rio de Janeiro, Brazil, 2009.

[23] Saygı, E., Master of Science Thesis, "Design, Construction and Testing of an Experimental Turbojet Engine", METU 1996.

APPENDIX A

UNCERTAINTY ANALYSIS

Errors can be classified as random errors and systematic errors. Random errors are caused from statistical fluctuations in the measured data. Systematic errors are generally results of measurement instruments. Random errors can be detected easily and reduced by increasing the measurement number while systematic errors cannot be detected easily and analyzed statistically.

Average measurement is given by;

$$\bar{x} = \frac{x_1 + x_2 + \ldots\ldots x_n}{N} \quad \text{(A.1)}$$

where N is total measurement number and x_1 and x_n are the measured values.
Standard deviation is given by;

$$S.D. = \sqrt{\frac{\sum(x_i - \bar{x})}{(N-1)}} \quad \text{(A.2)}$$

Precision error which is result of measurements can be calculated as;

$$P.E. = \frac{2 \times S.D.}{\sqrt{N}} \quad \text{(A.3)}$$

Total uncertainty is sum of bias error caused from systematic errors and precision errors. In other words, uncertainty includes both accuracy and precision. Total uncertainty is given as;

$$U = \pm\sqrt{B.E.^2 + P.E.^2} \quad \text{(A.4)}$$

APPENDIX B

2-D VELOCITY DISTRIBUTION

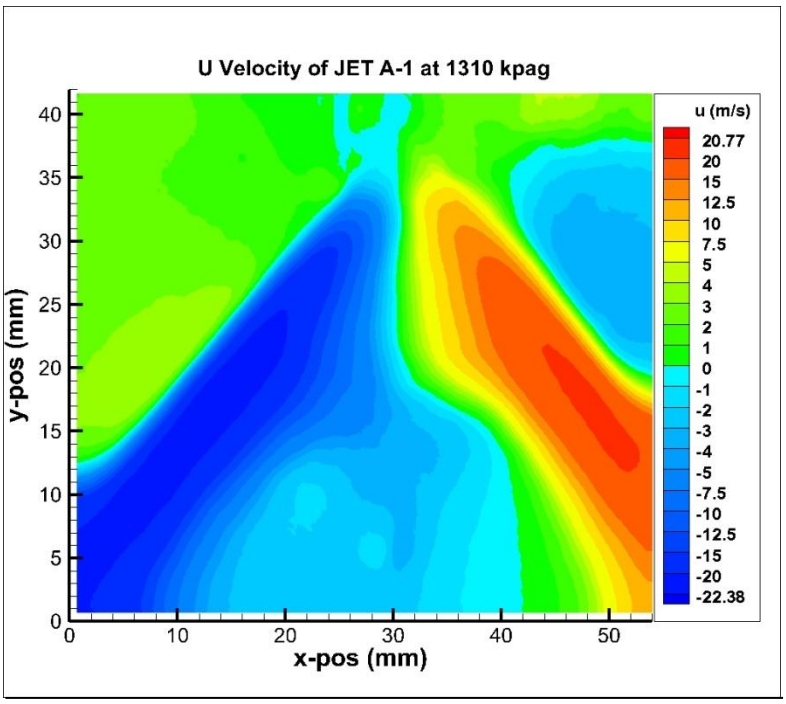

Figure B-1 U Velocity of JET A-1at 1310 kpag 1st Window

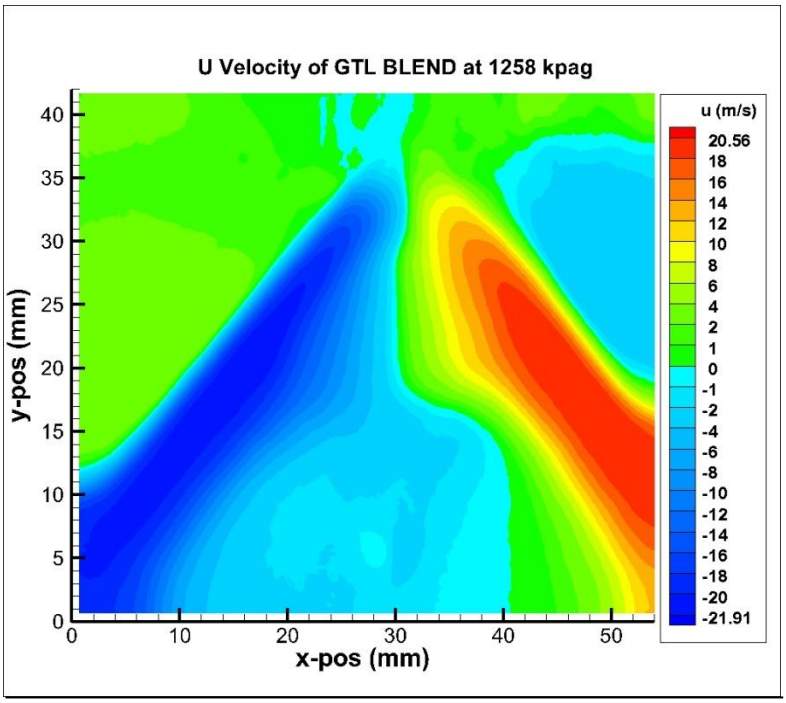

Figure B-2 U Velocity of GTL Blend 1258 kpag 1st Window

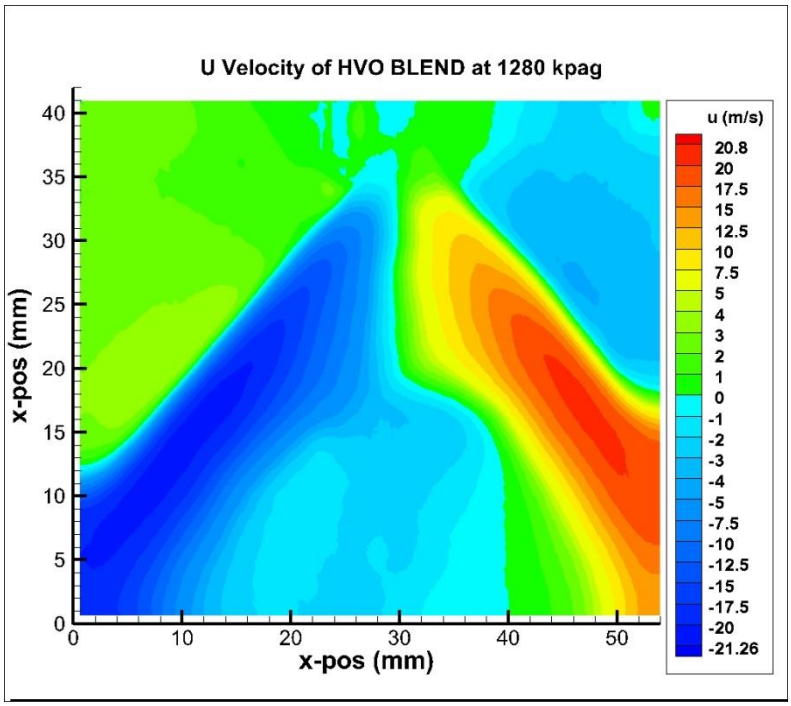

Figure B-3 U Velocity of HVO Blend 1280 kpag 1st Window

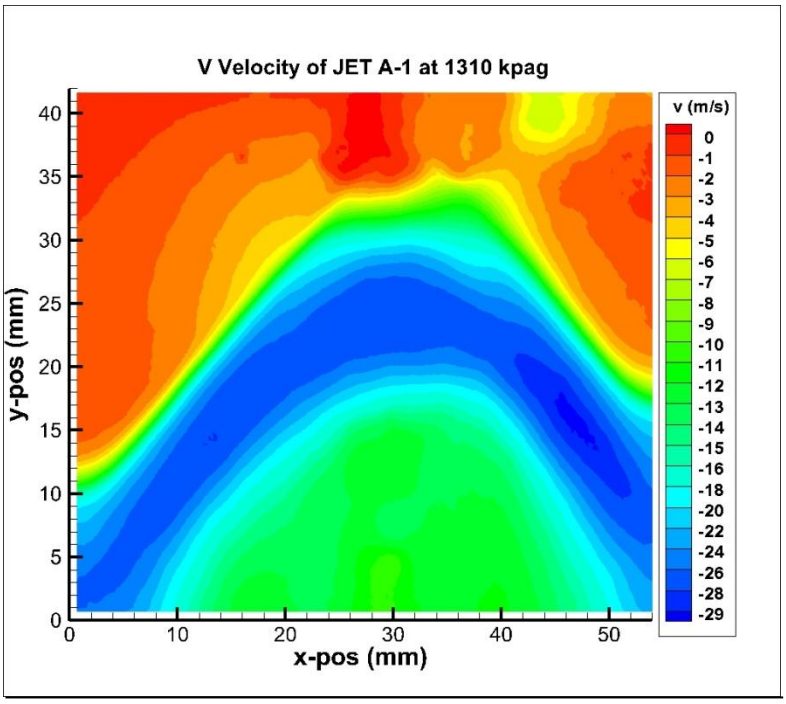

Figure B-4 V Velocity of JET A-1 1310 kpag 1st Window

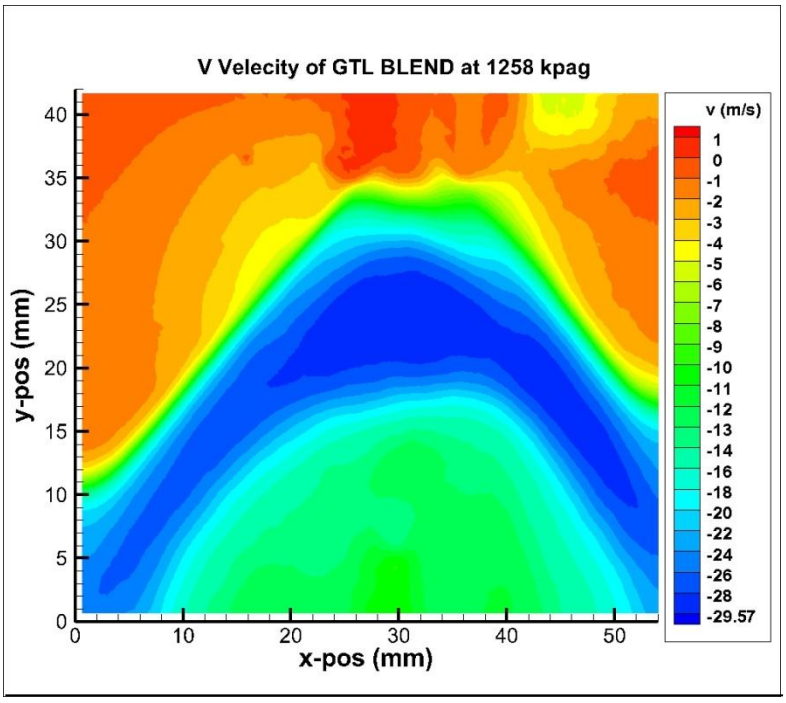

Figure B-5 V Velocity of GTL Blend 1258 kpag 1st Window

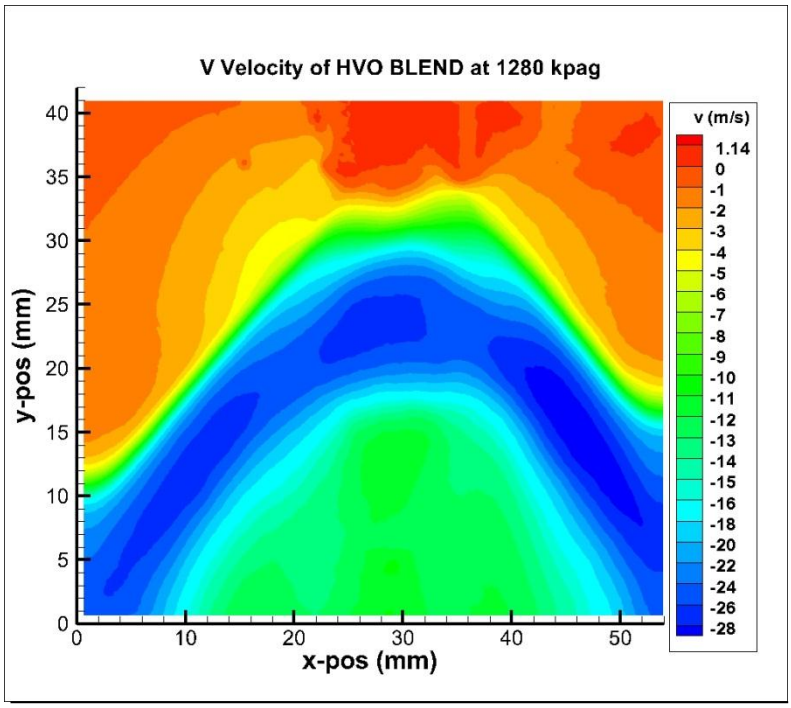

Figure B-6 V Velocity of HVO Blend 1280 kpag 1st Window

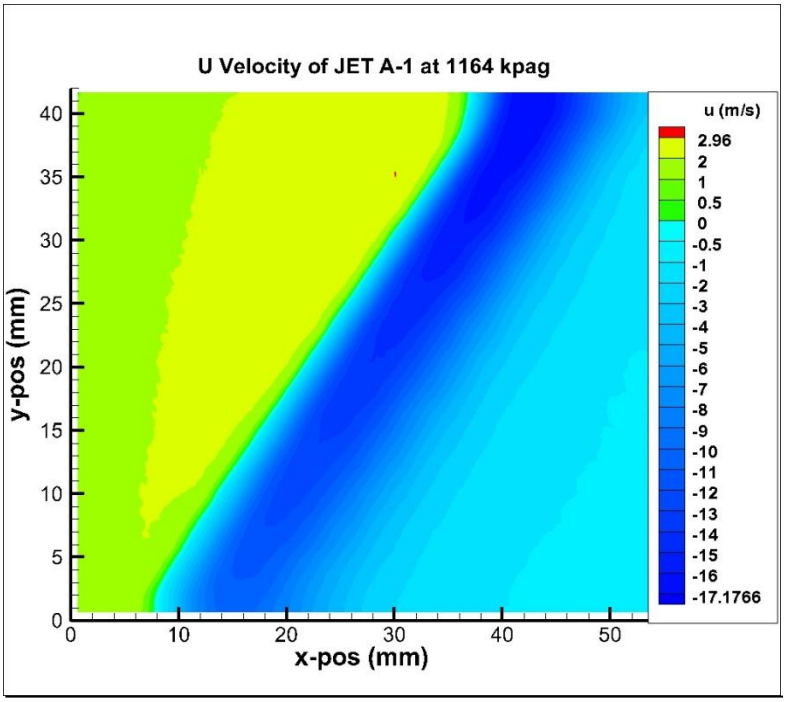

Figure B-7 U Velocity of JET A-1 1164 kpag 2nd Window

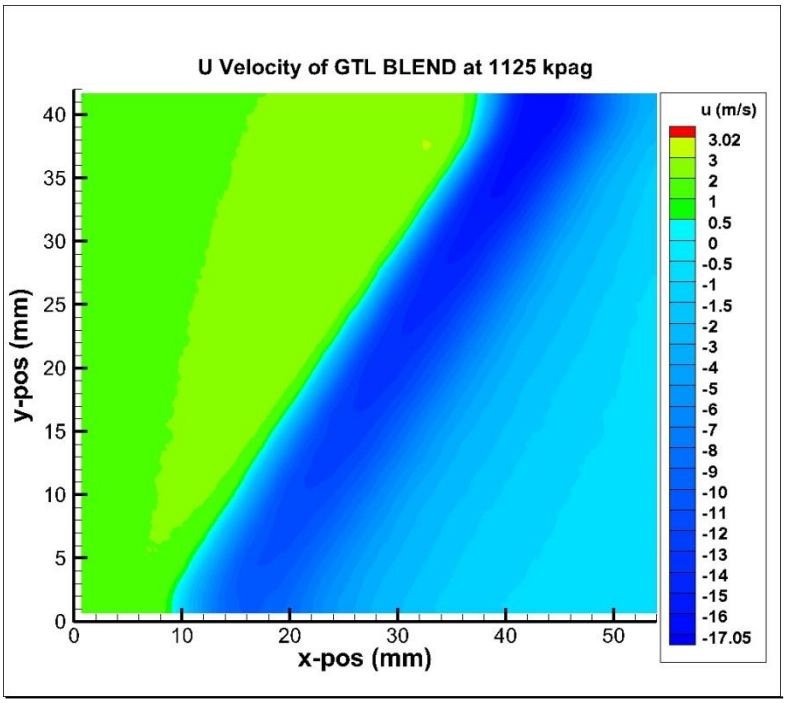

Figure B-8 U Velocity of GTL Blend 1125 kpag 2nd Window

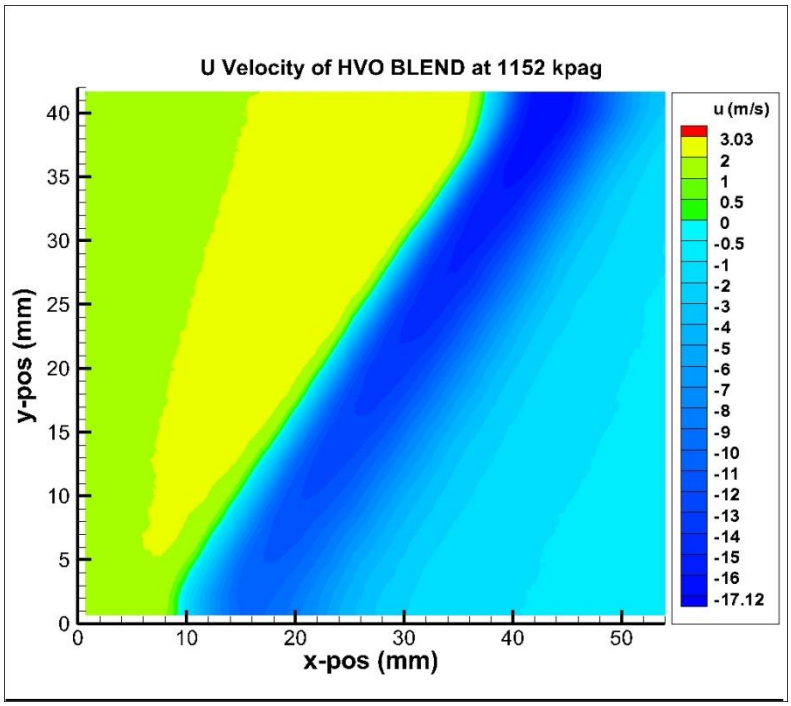

Figure B-9 U Velocity of HVO Blend 1152 kpag 2nd Window

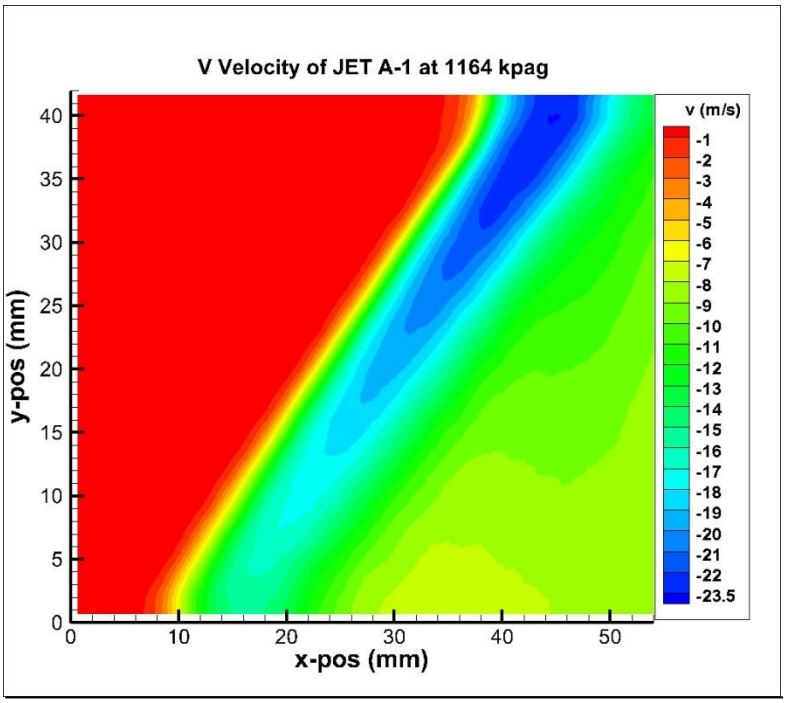

Figure B-10 V Velocity of JET A-1 1164 kpag 2nd Window

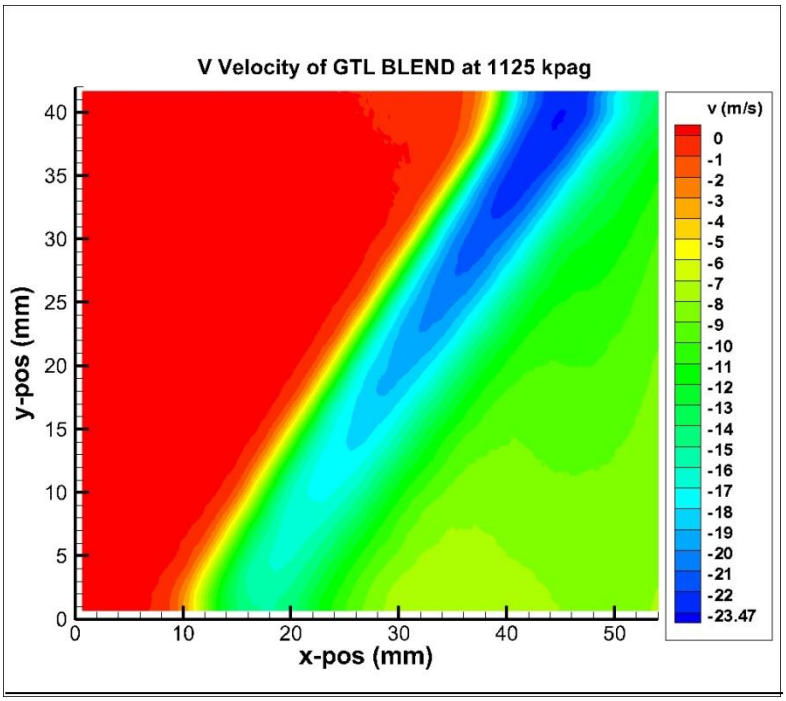

Figure B-11 V Velocity of GTL Blend 1125 kpag 2nd Window

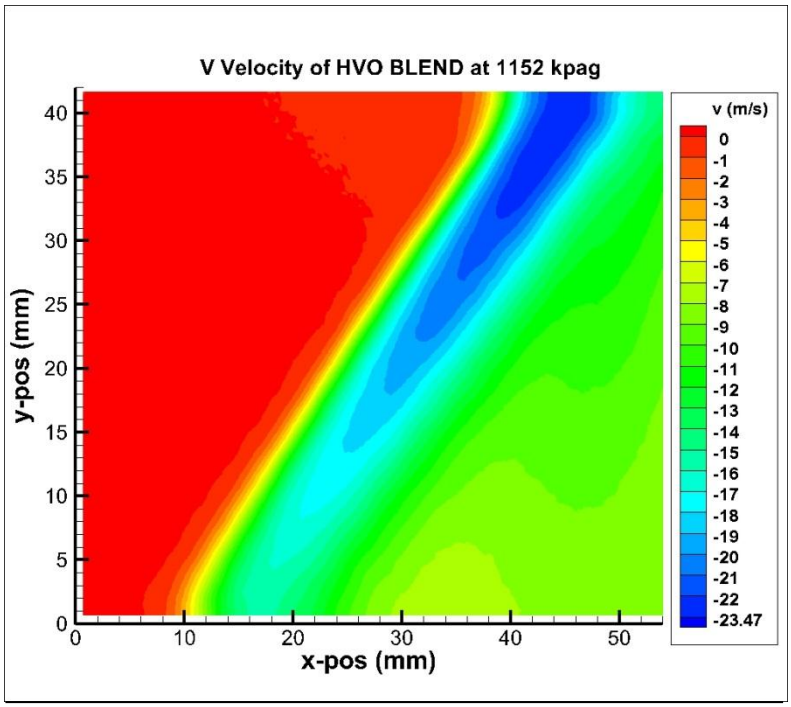

Figure B-12 V Velocity of HVO Blend 1152 kpag 2nd Window

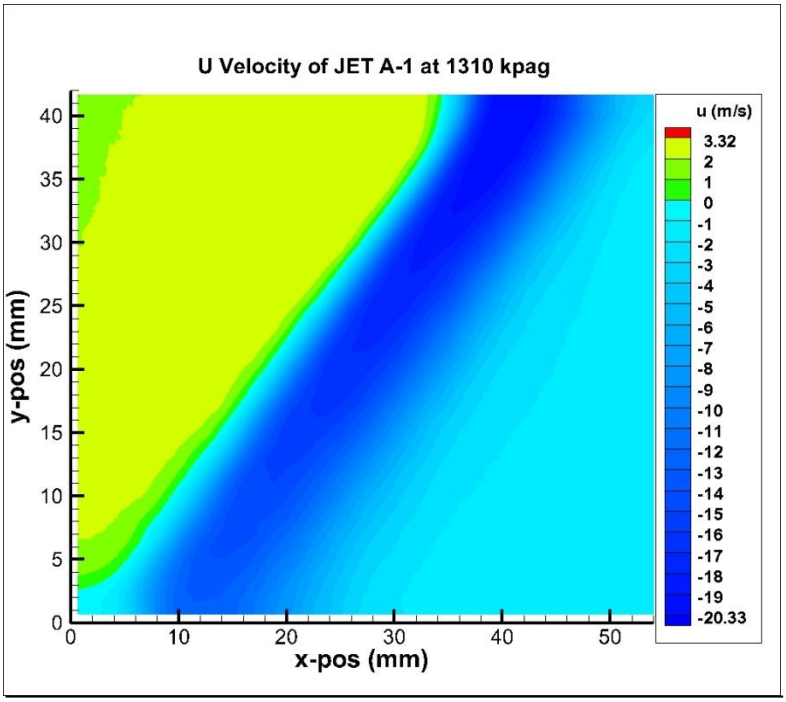

Figure B-13 U Velocity of JET A-1 1310 kpag 2nd Window

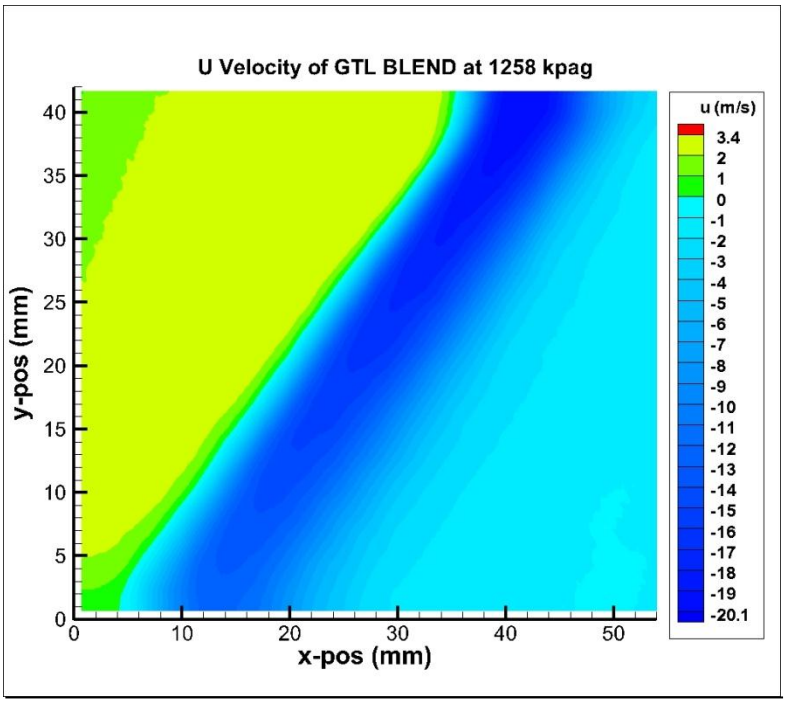

Figure B-14 U Velocity of GTL Blend 1258 kpag 2nd Window

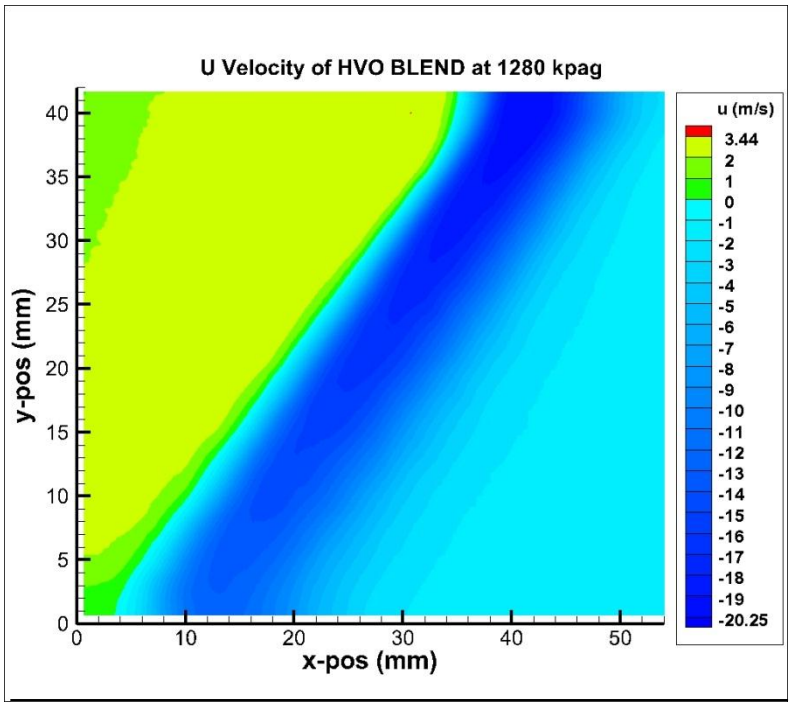

Figure B-15 U Velocity of HVO Blend 1280 kpag 2nd Window

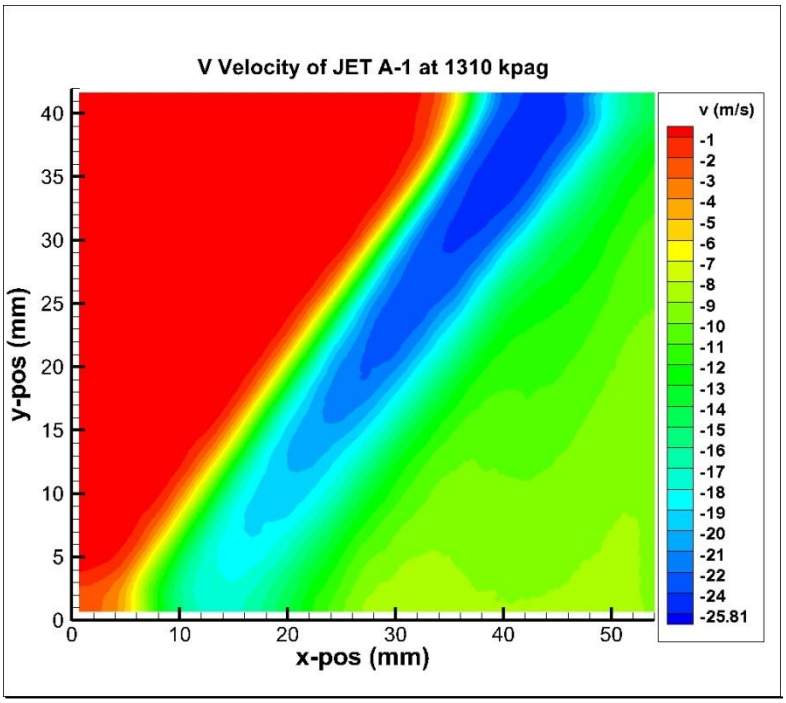

Figure B-16 V Velocity of JET A-1 1310kpag 2nd Window

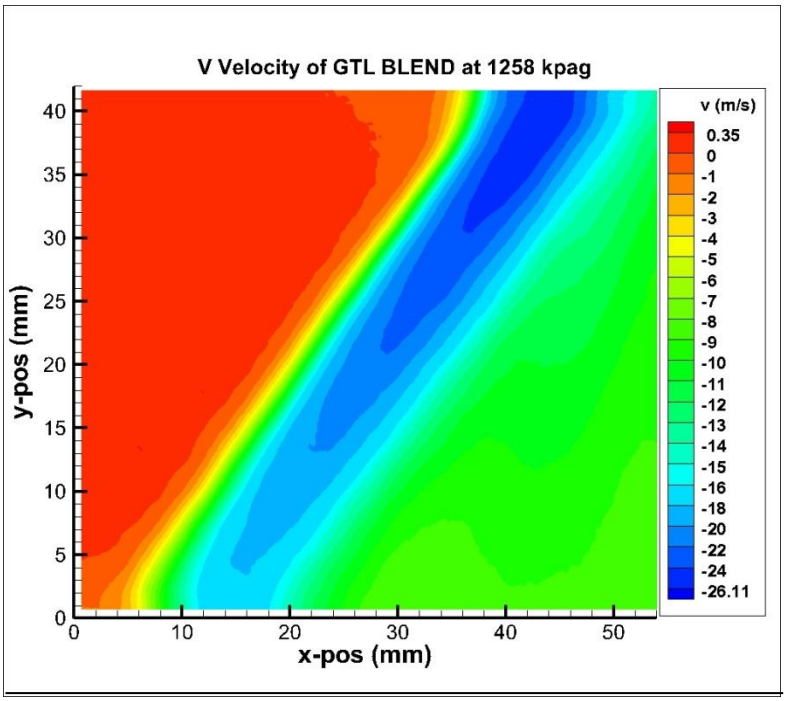

Figure B-17 V Velocity of GTL Blend 1258 kpag 2nd Window

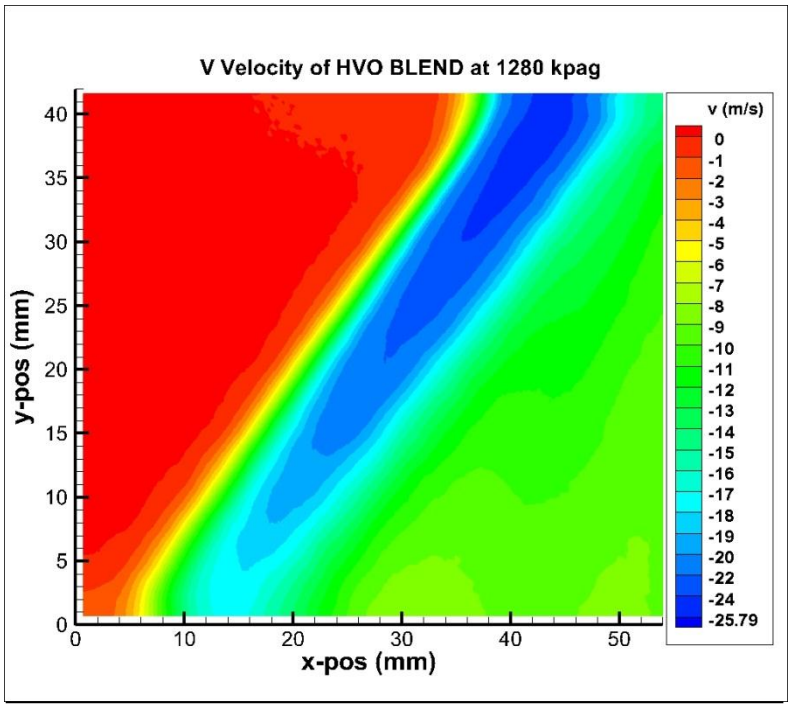

Figure B-18 V Velocity of HVO Blend 1280 kpag 2nd Window

APPENDIX C

JET A-1 FUEL PROPERTIES

Table C.1 Properties of JET A-1 Fuel

Analysis	Unit	Result	ASTM D1655 (JET A-1) Min	Max
-Density at 15 ºC	kg/m^3	791,0	775	840
-Appearance	-	Clear and Bright	Clear, Bright	
-Distillation				
Initial Boiling Point	ºC	150.6	-	
%10	ºC	165.2	-	205
%50	ºC	187.2	-	-
%90	ºC	224.4	-	-
End Boiling Point	ºC	251.0	-	300
Residue	%(v/v)	1.0	-	1.5
Loss	%(v/v)	0.8	-	1.5
-Flash Point	ºC	41.5	38	-
-Mercaptan Sulphur	%(m/m)	0.0004	-	0.003
-Sulphur	%(m/m)	0.001	-	0.30
-Viscosity at (-20 ºC)	mm^2/s	3.392	-	8
-Calorific Value	Mj/kg	43.42	42.8	-
-Hyrocarbon Types	%(v/v)	12.2	-	25

(Aromatics)			
-(JFTOT) Thermal Stability			
Control Temp. 260 ºC (min)	mL mm		
Filter Press. Dif. Tube	Hg		- 25
Deposit Rating	Visual		- 3